Structures 54 (2023) 89–105

Contents lists available at ScienceDirect

Structures

journal homepage: www.elsevier.com/locate/structures

Deterministic and probabilistic-based model updating of aging steel bridges

B. Barros, B. Conde, M. Cabaleiro, B. Riveiro *

CINTECX, Universidade de Vigo, GeoTECH Group, Campus Universitario de Vigo, As Lagoas, Marcosende 36310 Vigo, Spain

ARTICLE INFO

Keywords:
Aging steel bridge
Multidisciplinary experimental characterization
Surrogate modeling
Sensitivity analysis
Model updating

ABSTRACT

Numerical modeling is a very useful tool in different fields of bridge engineering, such as load-carrying capacity assessment or structural health monitoring. Developing a reliable computational model that accurately represents the actual bridge mechanical behavior entails advanced FEM-based modeling complemented by a comprehensive experimental campaign that provides the necessary supporting information and allows validating simulation outcomes. This paper proposes a unified approach aimed at the experimental characterization and FE model updating of aging steel bridges. It first involves the realization of an extensive experimental campaign aimed at the bridge's geometrical, material, and dynamic behavior characterization. Then, a model calibration framework is developed, where deterministic (optimization) and probabilistic (Bayesian inference) approaches are employed, and techniques such as global variance-based sensitivity analysis and Kriging-based surrogate modeling are further implemented in order to enhance the identification process and reduce the overall computational burden. The methodology has been validated in a historical riveted steel bridge in O Barqueiro, north of Galicia, Spain. The results show a good agreement in the identified model parameter values and a noticeable correlation between numerical and experimental modal properties, with an average relative error in frequencies of 0.34% and 0.44% for the deterministic and probabilistic approaches and an average MAC (Modal Assurance Criterion) ratio of 0.96.

1. Introduction

Bridges are one of the most critical assets within the terrestrial transport network. The design and construction of these structures are usually challenging due to the nature of their construction, with high heights and large spans to overcome, or the foundations on unstable soils in rivers or sea inlets. Bridges are usually the most expensive and vulnerable structures within the transport network [1].

For centuries, timber and stone bridges were the most frequent solution to overcome land obstacles, making it possible to communicate among isolated places and facilitate commercial routes worldwide [2]. After the industrial revolution and the consequent advance in metallurgy, the construction of many steel bridges was promoted [3]. Many of these ancient steel bridges continue in operation nowadays. These structures are generally subjected to adverse environmental effects that lead to decay, such as corrosion. The lack of proper maintenance and aging of bridges is a widespread problem affecting transport networks almost all over the world; e.g., in EEUU, 42% of bridges are over 50 years, and 7.5% are considered structurally deficient [4]. This issue calls for special attention to diagnosing structural integrity, safety analysis, and prognosis of remaining service life.

Numerical modeling is a powerful tool for model-based structural health monitoring and reliability-based structural assessment that can contribute to optimizing maintenance planning and costs [5–7]. This fact increases the interest in disposing of numerical models that faithfully represent the structural behavior according to the current bridge condition state. Among others, the lack of data regarding the material properties, the uncertain behavior of the connections, imprecise boundary conditions, or the existing damage might provoke discrepancies between the computational model predictions and the actual structural system response [8]. Therefore, numerical models must be tuned in a procedure known as FE model updating or model calibration [9], an inverse approach where uncertain model parameters that can often not be directly measured are estimated by adapting simulation model results to the actual measurements of the mechanical response [10].

Ancient bridges usually require obtaining a significant amount of data to perform accurate numerical modeling. Thus, the deployment of extensive experimental characterization campaigns is needed, where the synergetic use of different testing techniques [11–15] together with

* Corresponding author.
E-mail address: belenriveiro@uvigo.gal (B. Riveiro).

https://doi.org/10.1016/j.istruc.2023.05.020
Received 9 January 2023; Received in revised form 23 April 2023; Accepted 6 May 2023
Available online 19 May 2023

measurements of the static or dynamic response of the structure [16,17], are a crucial factor. Moreover, in the particular case of heritage constructions, non-destructive methods are usually preferred as they do not alter their original state [18,19]. Accordingly, in the existing literature, several works can be found where in-situ multidisciplinary surveys based on non-destructive testing are proposed to perform a proper FEM-based numerical modeling [20–22]. Nonetheless, these procedures, although relatively frequently executed in masonry or concrete bridges, are still scarcely adopted in the case of ancient steel bridges, where only visual inspections and ambient vibration testing are typically employed [23–25].

Multiple FE model updating strategies have been developed, which, aside from manual [26] and direct updating methods [27,28] can be roughly classified into (automatic iterative) deterministic and probabilistic approaches. Deterministic methodology refers to classical optimization methods, the most extensively adopted in the state of practice. Thus, a vast number of studies can be found in the existing literature using: i) global optimizers, such as genetic algorithms [24,29], particle swarm [25], evolutionary strategies [17], harmony search [30], or pattern search [31], ii) local optimization algorithms such as the trust-region reflective algorithm [20,21], iii) hybrid local–global optimization algorithms, such as genetic algorithm and improved cuckoo search (HGAICS) [32], or unscented Kalman filter and harmony search (UKF-HS) [33], and iv) surrogate-assisted strategies [34], to mention a few. In this regard, the reader is referred to [10] for a thorough review of the different FE model updating methods and related works. Alternatively, probabilistic methodologies based on Bayesian inference procedures can be employed [35], which have gained increased attention and have experienced significant development in recent years. Thus, in the literature, several research studies can be found using different techniques, such as Markov Chain Monte Carlo (MCMC) with Metropolis-Hastings algorithm [36,37], Hamiltonian Monte Carlo algorithms [38,39], Transitional MCMC [40,41], Gibbs based approach [42], Multi-resolution Bayesian non-parametric general regression method (MR-BNGR) [43], Approximate Bayesian Computation (ABC) methods [44,45], or Variational Bayesian methods [46,47], among others. For a more exhaustive review of the state-of-the-art, the reader is referred to [10,48]. Both approaches, deterministic and probabilistic, have pros and cons, see [49], but the combined use can provide valuable insight into the robustness of the FE model updating results. Accordingly, the joint employment of both methodologies has been recently tackled in some works [50,51]. In the bridge field, however, these studies are still scarce [52,53], especially in the case of aging steel bridges. Moreover, apart from updating algorithms, there is the need to integrate additional methods such as sensitivity analysis and surrogate modeling for a comprehensive and efficient FE model updating workflow that guides in the selection of the most important calibration parameters and allows for reducing computing time and computational resources.

This work proposes a unified approach aimed at the experimental characterization and FE model updating of aging steel bridges, encompassing a multidisciplinary experimental campaign aimed at the bridge's geometrical, material, and dynamic behavior characterization and a model calibration framework where deterministic (optimization) and probabilistic (Bayesian inference) approaches are employed together with techniques such as global variance-based sensitivity analysis and Kriging-based surrogate modeling to enhance the identification process and reduce the overall computational burden. The feasibility of the methodology has been validated in a historical riveted steel bridge in O Barqueiro, north of Galicia, Spain. The paper is organized as follows: Section 1 is the introduction, where the motivation of the study is presented. Section 2 describes the O Barqueiro bridge, including a brief historical background and details of its structural configuration. Section 3 describes the experimental campaign with details of the non-destructive tests performed and the corresponding results. Section 4 details the FEM-based modeling procedure. Sections 5, 6, and 7 present the different stages of the model calibration framework, i.e., sensitivity analysis, optimization-based model updating, and Bayesian calibration, including an outline of the theoretical background and a discussion of the obtained results. Finally, the conclusions are drawn in Section 8.

2. O Barqueiro bridge

O Barqueiro bridge is a riveted steel bridge located at the mouth of the Sor river between the municipalities of O Mañon (A Coruña) and O Vicedo (Lugo) in the northern region of Galicia, Spain. Downstream and upstream views of the bridge can be seen in Fig. 1. The original design dates from 1880, but this project was never realized [54]. Thus, the project was redesigned in 1894 with some modifications that affected the masonry abutments and piers, being the latter grounded at a depth of 20 m to overcome the problems related to the foundations at the sandy riverbed. The construction finally started in 1895 and was finished in 1901 [54].

The bridge is in a coastal zone characterized by high environmental salinity and strong winds. Thus, due to its degradation and decay, in the 80 s, the bridge was closed to the passing of cars and trucks. After some years of abandonment, in 2006, rehabilitation works were performed, and the structure was pedestrianized. O Barqueiro Bridge is currently listed as an asset of cultural interest in Galicia, thus emphasizing its high heritage value. Therefore, structural health monitoring and proper maintenance are essential to ensure its conservation.

O Barqueiro bridge is a three-isostatic-span steel arch bridge, each with a length of 48.10 m, a width of 6.40 m, and a height of 7.50 m, see Fig. 2. On each side, the arch rib has a parabolic shape, and its vertically linked to the tie girder through twelve vertical hangers and longitudinally by forty-four rectangular-shaped cross bracings. Both arch ribs are connected through six sway systems, which in turn, are longitudinally linked by circular-shaped upper lateral bracings. On the other hand, the deck is formed by sixty-five stringers, equally divided into thirteen panels of five members each, and fourteen cross-girders, originally supporting the road pavement and, after rehabilitation, wooden planks. Circular-shaped lower lateral bracings are also arranged between the third and the eleventh panels. On each span, the bridge presents simple supports on one side and roller supports on the other. Some details of the bridge's structural configuration can be seen in Fig. 3.

All original structural members were built-up using steel plates and L-type profiles joined by rivets. Thus, the cross-girders and stringers present an I-shaped cross-section composed of a web plate riveted to four angles that constitute the flanges. The arch ribs and tie girders have a similar cross-section shape, with an additional plate attached to the flanges. The cross-girders and central stringers have additional reinforcement steel plates on the top and bottom sides to increase flexural capacity. The vertical hangers are made of two T-shaped profiles joined by lacings. As for the sway systems, these are formed by struts made of double angles and rectangular-shaped bracings. A detailing of the different cross-section shapes is given in Fig. 4.

3. Experimental campaign

The experimental campaign was carried out in two different stages. The first stage involved the visual inspection, geometrical characterization through on-site measuring and terrestrial laser scanning survey, and ultrasonic testing for estimating steel elastic properties. The second stage corresponded to an ambient vibration test to determine the experimental modal properties.

3.1. Visual inspection

An in-depth field survey was performed to determine the current condition state of the bridge. The site inspection addressed two main issues: i) elaborating a damage mapping; ii) analyzing the retrofitting actions performed during rehabilitation.

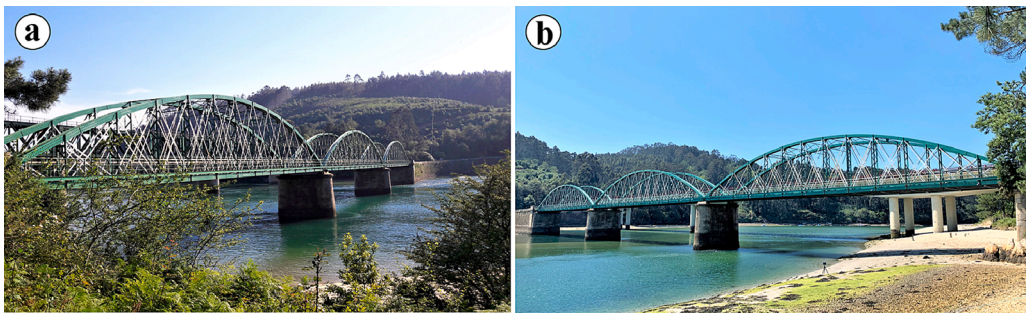

Fig. 1. Downstream (a) and upstream (b) views of O Barqueiro bridge.

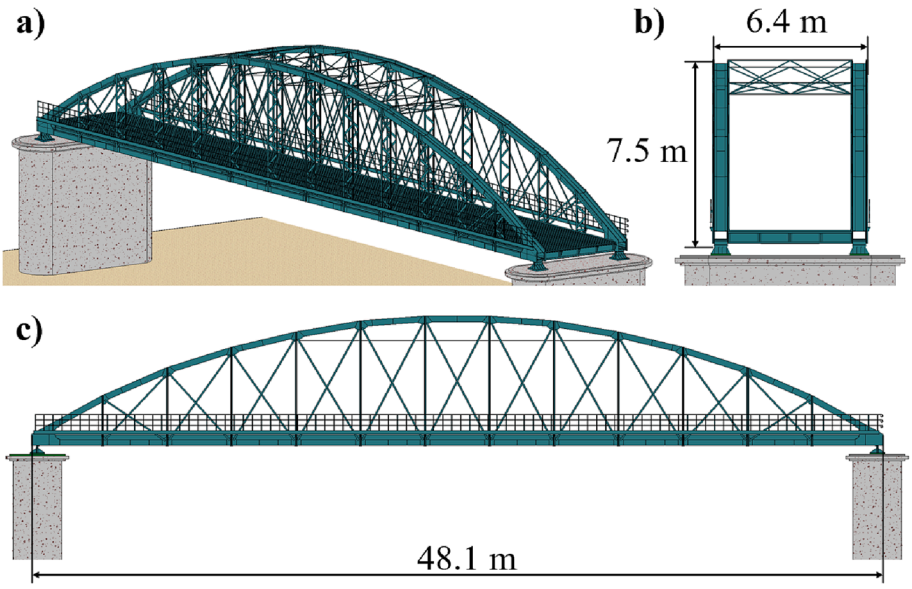

Fig. 2. O Barqueiro bridge: a) isometric view (b) cross-section and (c) elevation view.

Fig. 3. Details of O Barqueiro bridge: a) arch ribs, vertical hangers, sway systems, and cross bracings b) tie girders, cross-girders, and stringers c) supports.

Regarding the former, the following problems were identified: a) the bridge is located in a highly corrosive environment; thus, general corrosion is present almost throughout the structure; b) the presence of dimples and pitting at various elements; c) thickness losses at some elements, such as the cross-girders and stringers; d) detachment due to the absence of rivets, holes, and lack of material at some local areas of the stringers flanges; e) delamination of steel members at some of the riveted connections between the tie girders, cross-girders, and vertical hangers; f) lack of rivets at some of the connections of the stringers with the cross-girders; g) partial detachment due to the absence of rivets of the flexural reinforcement plates; h) deposition of organic residues at the web of the arch and tie girders; i) water and moisture retention in the wood strips in contact with cross-girders and stringers; j) poor condition of the steel protective coating. Some details of all the issues mentioned above can be observed in Fig. 5.

As for the steel connections between tie girders, cross-girders, and vertical hangers, given their relevance in the bridge mechanical behavior, a comprehensive individual inspection was carried out, after which a qualitative classification of their damaged condition state was elaborated, see Fig. 6, grouping them into two major categories: a) slight-to-moderate damaged and b) high damaged connections.

In the rehabilitation of 2006, the following actions were undertaken:

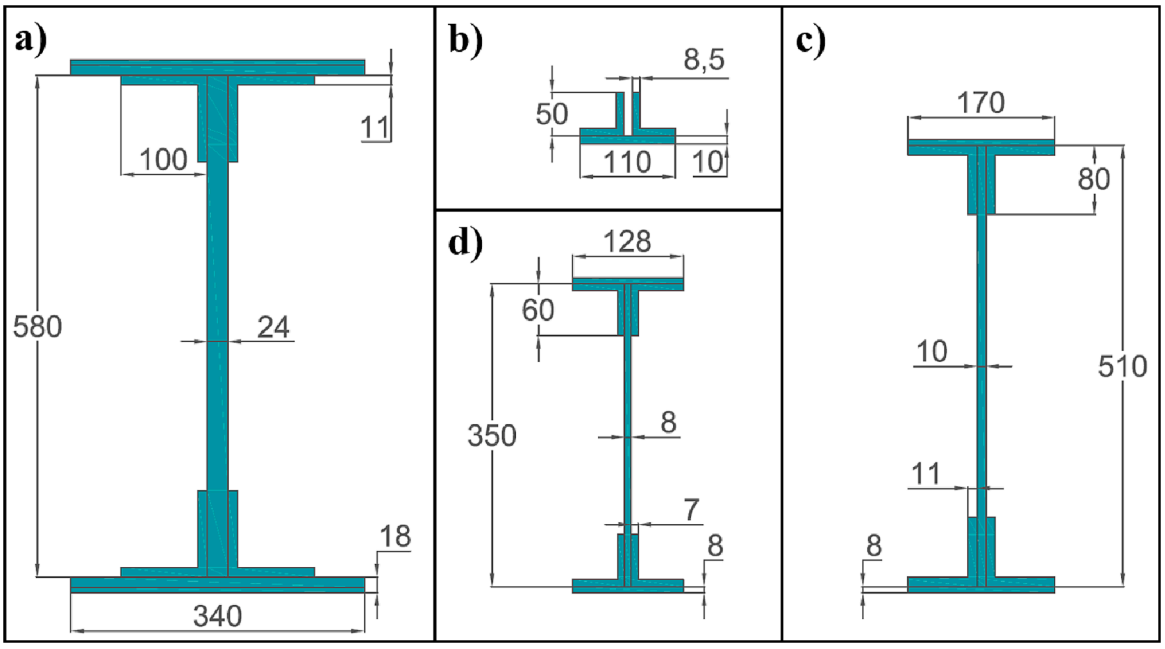

Fig. 4. Cross-section shape and dimensions of steel members: a) arch ribs and tie girders b) vertical hangers c) cross-girders d) stringers.

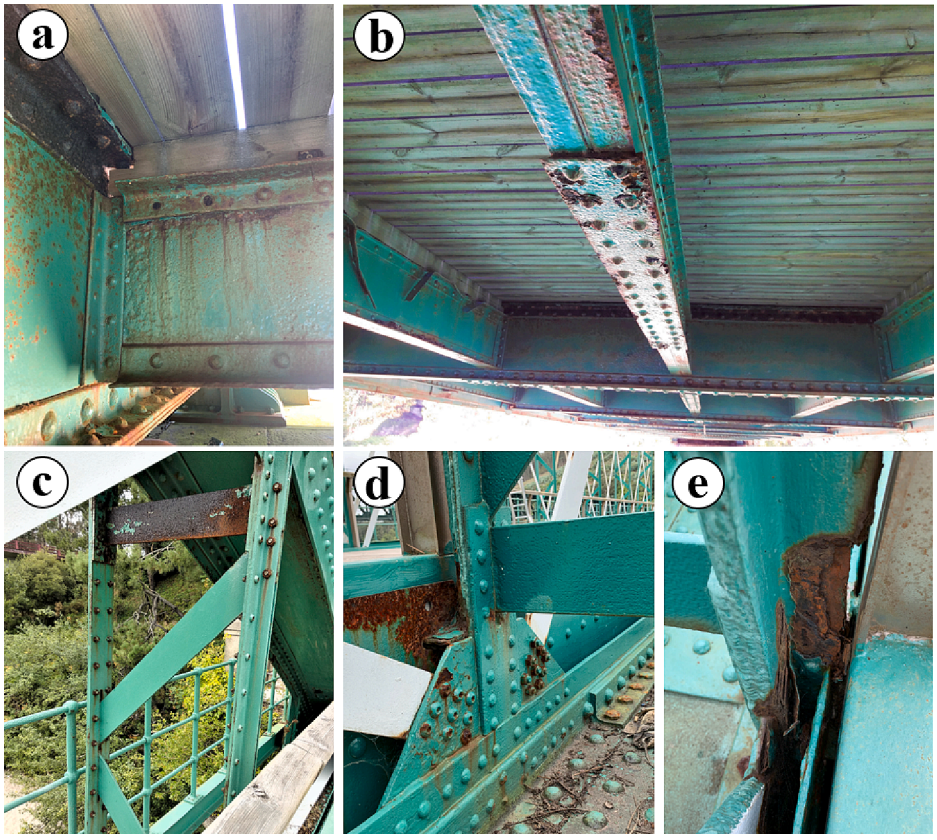

Fig. 5. Examples of damaged and retrofitted elements in O Barqueiro bridge: a) Lack of rivets in a stringer b) detachment of the flange plates c) rivets replaced by bolts d) retrofitted hanger e) corrosion in the lower part of a hanger.

a) the pavement was replaced by a timber system formed by wooden strips and planks; b) cantilever sidewalks were removed; c) original railings were attached to the vertical hangers in the outer side; d) a new steel and wood railing was installed on the inner side; e) twenty-six cross-bracings and twelve vertical hangers were partially replaced or retrofitted; e) a significant amount of rivets were replaced by bolts; f) cleaning and painting of the whole structure. It is worth noting that new L-type sections were employed for the replaced vertical hangers connected to the original elements by welding. A few years later, these new profiles present an advanced corrosion state with considerable

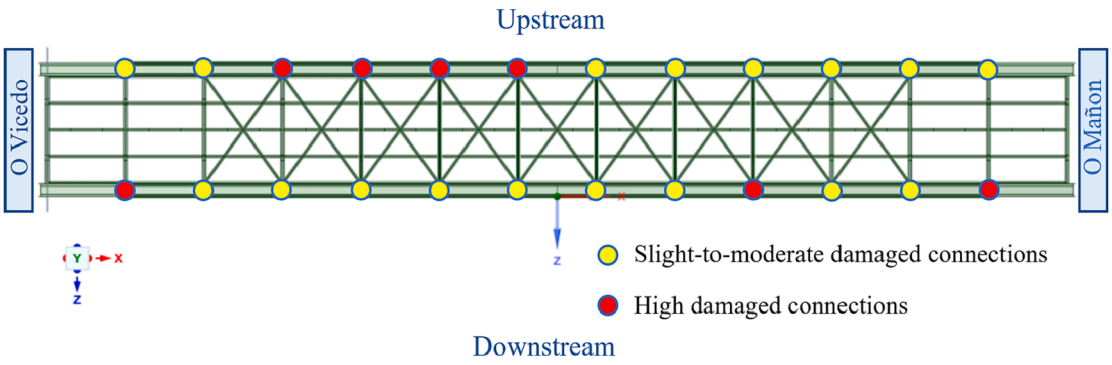

Fig. 6. Damage mapping of the deck steel connections.

delamination and material loss, see Fig. 5.

3.2. Terrestrial laser scanning survey and on-site measuring

A Terrestrial Laser Scanning (TLS) survey was performed to obtain an accurate 3D digitalization of the structure that provides precise information about the main bridge dimensions, the assembly detailing of the structural elements, or various relevant geometric features such as the shape and dimensions of gusset plates, among others [55–57]. The equipment was a phase-shift terrestrial laser scanner FARO Focus 3D x130 [58]. Ten scans from different positions were taken to characterize the overall geometry of the bridge. Four scan positions were under the deck, while the remaining ones were on the deck. The original point clouds had around 20 million points each. After aligning all the scans to the same reference system, the consolidated point cloud was post-processed to filter undesirable features such as vegetation or sand. The final 3D digitalization comprises around 12 million points. Fig. 7 shows one of the positions of the TLS under the deck and the 3D visualization of the corresponding point cloud.

Complementary to the LiDAR data, in-situ manual measurements aimed at characterizing the net cross-section and thickness variability of the different steel members were also collected during the on-site inspections. Accordingly, a precision gauge with a tolerance of ± 0.01 mm was employed, obtaining a total of 325 values spread over the main members (arch ribs and tie girders, vertical hangers, cross-girders, etc.) and on different regions (i.e., angles and steel plates). The (rounded) average values of these experimental measurements are summarized in Table 1; see also Fig. 4.

Table 1
Dimensions of the main steel members as obtained from on-site measuring.

Element	Region	Dimensions (mm)
Arch ribs/Tie girders	Flange thickness	18
	L-shaped profile thickness	11
	Web thickness	24
Vertical hangers	Plate thickness	10
	L-shaped profile thickness	8.5
	Lacings thickness	10
Stringers	Reinforcement plate	8
	L-shaped profile thickness	7
	Web thickness	8
Cross-girders	Reinforcement plate	8
	L-shaped profile thickness	11
	Web thickness	10
Rectangular-shaped cross bracings	Height	90
	Width	10
Circular-shaped upper and lower lateral bracings	Radius	10

3.3. Ultrasonic testing

Laboratory testing, such as uniaxial tensile tests on specimens extracted from the structure, is the usual way for material properties characterization. However, in the case of heritage structures, testing procedures are constrained by the non-intrusion principle. Thus, non-destructive in-situ testing techniques are alternatively adopted in this type of intervention. Accordingly, a non-destructive method, ultrasonic testing, was employed in this study to estimate the steel elastic properties, particularly the Young's modulus.

This material property can be obtained by measuring the propagation velocity of the mechanical (longitudinal and transversal) waves in the steel [59]. The relationship between the Young's modulus (E) and the velocity of transversal waves (c_t) can be expressed according to Equation (1), where μ is the Poison's ratio, and ρ is the density of the steel.

$$E = 2\rho c_t^2(1+\mu) \quad (1)$$

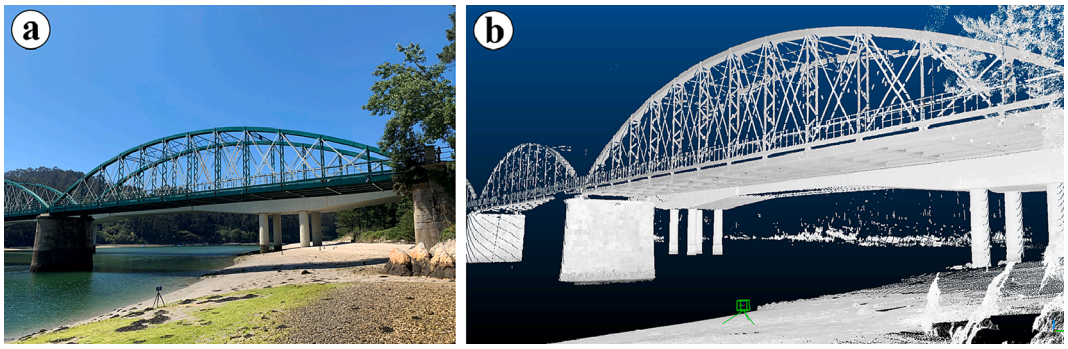

Fig. 7. TLS survey and example of an acquired point cloud.

Both velocities are related by the Poisson's ratio, as shown in Equation (2):

$$\mu = \frac{\frac{1}{2} - \left(\frac{c_t}{c_l}\right)^2}{1 - \left(\frac{c_t}{c_l}\right)^2} \tag{2}$$

Combining Equations (1) and (2), the Young's modulus can also be related to the velocity of propagation of the longitudinal waves (c_l) as follows:

$$E = \frac{\rho c_l^2 (1+\mu)(1-2\mu)}{1-\mu} \tag{3}$$

The equipment employed to perform the test comprised an ultrasonic thickness gauge model MX-3 of Dakota ultrasonics [60] and a high-precision digital gauge. These two devices were used to measure the velocity of propagation of the longitudinal waves (c_l) according to the following two-step procedure: i) first, the thickness of the tested steel (plate) element is measured with both devices; ii) then, the measurement obtained by the digital gauge is employed to correct the one obtained with the ultrasonic device, thus returning c_l. This process was performed in sixty-six different bridge areas, only on single plates and non-damaged areas, replicating each measurement point five times. As a result, a significant amount of measurements was obtained (330), yielding a Young's modulus with a mean value of 188.94 GPa and a Coefficient of Variation (CoV) of 5.24%. The maximum and minimum values were 224.28 GPa and 173.46 GPa, respectively.

3.4. Ambient vibration testing

In the second stage of the experimental campaign, a dynamic identification based on an Ambient Vibration Test (AVT) was performed to determine the experimental modal properties (i.e., natural frequencies, mode shapes, and damping ratios) of the bridge. In order to establish the main conditions of the ambient vibration test (acquisition time, sampling rate, and location of the sensors), the numerical modal analysis results obtained with a preliminary FE model were used. Thus, it could be concluded that the first natural frequency was around 1.0 Hz (f_{min}) while frequencies of higher vibration modes were in the order of 10.0 Hz (f_{max}), so it was decided to set the sampling frequency (f_s) at 128 Hz, following the criterion in Ventura et al. [61]:

$$f_s > 2.4 f_{max} \tag{4}$$

On the other hand, to establish the acquisition time, different criteria can be selected according to the existing literature. Accordingly, L.F. Ramos mentions in [62] that by his own experience, 1000 times the highest natural period of interest is enough if the structure is well excited, while some other authors, such as Rodrigues et al. [63], consider the empirical rule of 2000 times the highest natural period of interest; in Ventura et al. [61], the acquisition time is established following Equation (5), where ç is the damping ratio. In this study, the acquisition time was fixed as 45 min per setup, thus complying with all the aforementioned criteria.

$$T_{tot} > \frac{20}{2çf_{min}} = \frac{10}{çf_{min}} \tag{5}$$

The equipment employed in the ambient vibration test was six uniaxial seismic accelerometers type 8340 with a sensitivity of 10 V/g and a frequency range of 0.1–1500 Hz, and an acquisition module type 3050 with a frequency range of 0–51.2 kHz, both of the Brüel & Kjaer company [64]. Steel supports in an L-shape format were ad-hoc designed and manufactured to fix the accelerometers to the structure with the help of magnetic anchors. Given the equipment constraints at the time of testing, namely due to the number of available accelerometers and mainly the length of the cables, a multi-setup test was designed where the reference sensors were fixed at the mid-center span to cover the whole bridge geometry satisfactorily (see Fig. 8). It should be noted that this arrangement is not ideal since placing the reference sensor in the central part of the bridge makes it impossible to characterize the vibration modes that have zero displacements there. During the design phase of the test, it was anticipated that two of the first six modes would not be captured due to this problem. However, due to the short length of the cables, any other approach would have resulted in monitoring only a portion of the structure, and in this sense, it was preferred to have measurement points distributed throughout the bridge.

Two reference accelerometers, fixed in the same position (point 11) during all the different setups, were employed to obtain the correlation matrix between the mobile and reference sensors thus avoiding non-stationarity conditions. A total of twenty-one setups were carried out, as summarized in Table 2, being the adopted positions in consonance with those areas where the main (lower) vibration modes presented meaningful modal displacements as obtained from FEM-based simulations. Accordingly, in Fig. 8, in blue is the position of the reference sensors; in red, the position of the mobile sensors placed in the tie girders; and in green, the position of the mobile sensors placed in the vertical hangers at a high of 3.0 m. At each point, accelerations in the vertical (Y) and transversal (Z) directions were recorded. During the test, the structure was subjected to environmental and operational loads such as wind and human walking.

Vibration data were analyzed with the software ARTeMIS Modal [65]. The records were processed using a decimated factor of 10 times, and modal parameters were determined by two different techniques, namely, the Enhanced Frequency Domain Decomposition (EFDD) [66] and the Stochastic Subspace Identification using the Principal Component algorithm (SSI-PC) [67,68]. A total of four vibration modes were identified; see Table 3 and Fig. 9. The first vibration mode is a lateral flexural mode shape of the whole bridge. The second vibration mode is a lateral flexural mode shape of the arch girders and the deck in counter phase. The third vibration mode is a vertical flexural mode of the whole bridge, and finally, the fourth vibration mode is a torsional mode shape. Given that the SSI-PC method shows slightly better results (less complexity), its outputs have been used as ground truth data for the subsequent FE model updating process.

4. Numerical modeling

4.1. Preliminary FE model

A 3D Finite Element (FE) model was developed based on the data obtained during the experimental campaign, particularly regarding the as-built geometry extracted from the point clouds and the on-site measurements. The modeling process was performed using the Diana FEA [69] and MATLAB [70] software packages. For geometrical modeling, line bodies were used to represent almost all bridge elements except for the arch ribs and tie girders, where a mixed modeling approach was adopted, using line bodies for the flanges and surface bodies for the web (see Fig. 10 a)).

For the mesh, first-order *Mindlin* beam elements were predominantly used for all steel members, except for the web of the arch ribs and tie girders, which in consonance with the abovementioned, were meshed using four-node quadrilateral, isoparametric shell elements. Moreover, the rectangular-shaped cross bracings and the circular-shaped lateral lower and upper bracings were meshed using two-node cable elements. Based on a mesh sensitivity analysis, the element dimension was set at 10 cm, except for the bracing systems meshed with only one element. Details of the FE mesh are given in Fig. 10 b).

The cross-section dimensions of the different steel members were defined in accordance with the experimental geometrical characterization, see Fig. 4 and Table 1. Given the non-standard shape of the built-up riveted members, cross-sectional properties were derived via numerical integration. On the other hand, to suitably replicate the actual structural configuration of the bridge, "offsets" from the CAD supporting lines

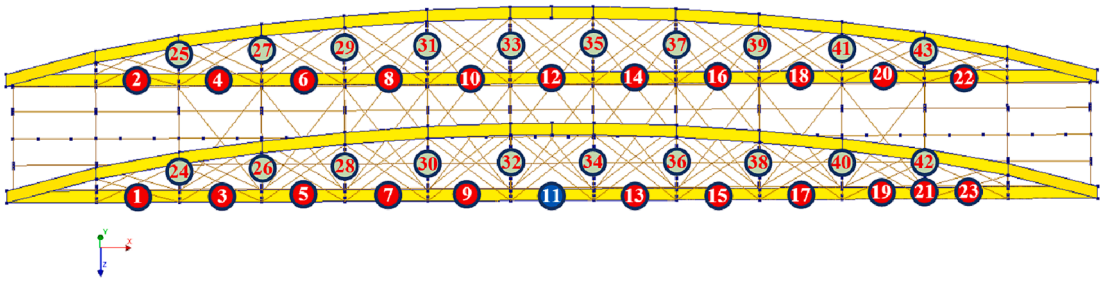

Fig. 8. Location of the sensors in the ambient vibration test.

Table 2
Overview of setups in the ambient vibration test.

Setup	Positions					
	Reference sensors		Mobile sensors			
	Sensor 1	Sensor 2	Sensor 3	Sensor 4	Sensor 5	Sensor 6
1	11 Y	11 Z	1 Y	1 Z	2 Y	2 Z
2	11 Y	11 Z	3 Y	3 Z	4 Y	4 Z
3	11 Y	11 Z	5 Y	5 Z	6 Y	6 Z
4	11 Y	11 Z	7 Y	7 Z	8 Y	8 Z
5	11 Y	11 Z	9 Y	9 Z	10 Y	10 Z
6	11 Y	11 Z	21 Y	21 Z	12 Y	12 Z
7	11 Y	11 Z	13 Y	13 Z	14 Y	14 Z
8	11 Y	11 Z	15 Y	15 Z	16 Y	16 Z
9	11 Y	11 Z	17 Y	17 Z	18 Y	18 Z
10	11 Y	11 Z	19 Y	19 Z	20 Y	20 Z
11	11 Y	11 Z	22 Y	22 Z	23 Y	23 Z
12	11 Y	11 Z	24 Y	24 Z	25 Y	25 Z
13	11 Y	11 Z	26 Y	26 Z	27 Y	27 Z
14	11 Y	11 Z	28 Y	28 Z	29 Y	29 Z
15	11 Y	11 Z	30 Y	30 Z	31 Y	31 Z
16	11 Y	11 Z	32 Y	32 Z	33 Y	33 Z
17	11 Y	11 Z	34 Y	34 Z	35 Y	35 Z
18	11 Y	11 Z	36 Y	36 Z	37 Y	37 Z
19	11 Y	11 Z	38 Y	38 Z	39 Y	39 Z
20	11 Y	11 Z	40 Y	40 Z	41 Y	41 Z
21	11 Y	11 Z	42 Y	42 Z	43 Y	43 Z

Table 3
Natural frequencies of the identified vibration modes.

Experimental mode	EFDD (Hz)	SSI-PC (Hz)
1	1.065	1.051
2	2.709	2.713
3	6.168	6.190
4	7.337	7.363

were introduced to represent the actual centroids' position. Other issues concern the timber deck, which was modeled as a dead load distributed on the cross-girders and stringers, and the mass of the gusset plates introduced in the form of point masses acting at the arch rib and tie girder joints.

With regards to the boundary conditions, the bridge presents roller bearings on the O Vicedo side (see Fig. 6); thus, displacements in the longitudinal direction (X-axis) and in-plane rotations were allowed (Z-axis), while on the O Mañon side, only rotations were allowed (pin bearings). For the steel properties, the average value of the Young's modulus estimated from ultrasonic testing was used as the first estimate with a density of 7850 kg/m3 and a Poisson's ratio of 0.3. For the numerical modal analysis, a two-step procedure was followed, where in the first step, the self-weight of the structure was introduced, mobilizing the stress-stiffening (geometric non-linearity) response of the bracing systems, and in the second step, the eigenfrequencies and eigenmodes were calculated.

This initial model was used to determine the main settings of the ambient vibration test. Once the experimental modal properties were identified, the adequacy of the numerical predictions was checked against the actual responses of the structure. Accordingly, Table 4 summarizes the relative errors between the numerical and experimental frequencies and the similarity between the mode shapes quantified by the Modal Assurance Criterion (MAC). The MAC ratios show a high correlation between numerical and experimental modal displacements with values generally above 0.90; however, discrepancies in the frequencies of the vibration modes can be observed. Thus, the need for a FE model updating process is underlined.

4.2. Model refinements

To represent the actual mechanical behavior of the bridge as accurately as possible and thus reduce the bias of the FE model, some refinements were implemented prior to the calibration process:

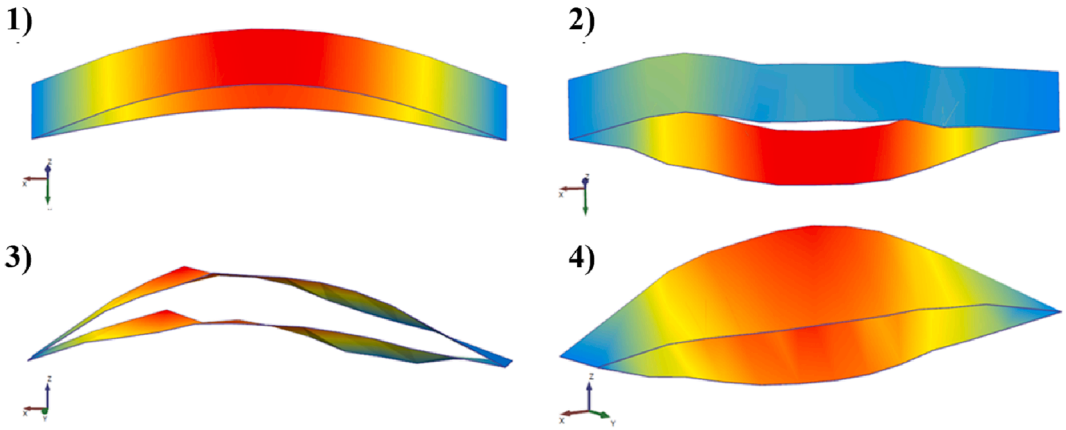

Fig. 9. Identified mode shapes from the output-only modal analysis.

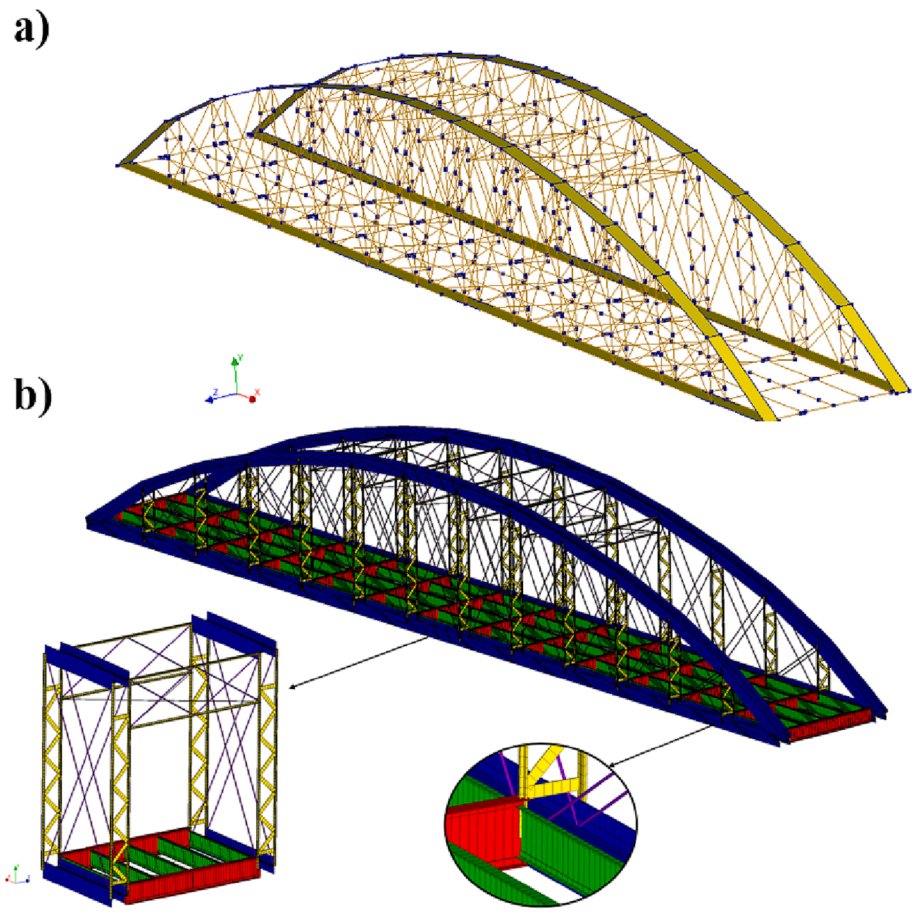

Fig. 10. Numerical model of O Barqueiro Bridge a) geometrical representation b) finite element mesh.

Table 4
Comparison between numerical and experimental modal results for the preliminary FE model.

Vibration mode	f_{exp}(Hz)	f_{num}(Hz)	Error (%)	MAC
1	1.051	1.212	15.32	0.99
2	2.713	3.041	12.09	0.89
3	6.190	6.471	4.54	0.93
4	7.363	8.748	18.81	0.98

- According to the field inspection and the elaborated damage mapping (Fig. 6) of the steel connections between vertical hangers, cross-girders, and tie girders, pinned joints were assumed for the highly damaged connections, while for the slightly to moderately damaged connections, rotational springs were introduced to allow the modeling of a semirigid behavior. Pinned or fully rigid behavior was considered for the rest of the FE model joints, depending on the particular constructive scheme.
- The aging of bridges causes deterioration in their supports that might lead to stiffness variation. This issue can be modeled by introducing artificial springs [71]. Accordingly, two translational springs in each support were implemented in the vertical (Y-axis) and transversal (Z-axis) directions.
- Corrosion leads to variation in the thickness dimensions of steel members, being indeed a spatial variation phenomenon. Initially, the average value of the experimental measurements (see Table 1) was adopted to represent the net cross-section adequately. However, given the stochastic nature of the problem, the finite number of experimental measurements performed, and the scattering observed, uncertainty regarding the members' thickness is still present. Thus, thickness dimensions were parameterized in the FE model for the different cross-sections (see Fig. 4). For this purpose, an algorithm was developed in MATLAB that automatically recalculates the cross-section profile coordinates as a function of the thicknesses, and for the resulting arbitrary shapes, the mechanical sectional properties (i.e., area, moments of inertia, Saint-Venant torsion constant, etc.) are calculated via numerical integration.

5. Sensitivity analysis

Before the FE model updating, a global variance-based sensitivity analysis was performed. This technique allows for identifying the subspace of the most influential input variables in the bridge modal responses, thus improving the efficiency and accuracy of the subsequent calibration process. Sobol' indices (ANOVA) [72] is the sensitivity analysis methodology employed in this work. This method provides a complete overview of the impact of each input parameter in terms of single and interaction effects by analyzing the model output variance. Its main drawback is the high number of simulation runs required, which implies a substantial computational burden. To circumvent this issue, an alternative approach is to build a surrogate model replacing the original FE model, thus obtaining sufficiently accurate results but with a much lower numerical effort. In the following, the search space for the different uncertain input parameters is presented, a brief background of the methods involved in the surrogate-assisted global sensitivity analysis, and a discussion of the obtained results.

5.1. Parameter ranges

The parameter ranges were established according to the existing

literature data and the experimental observations. Thus, concerning the steel properties, the density lower and upper bounds were established following the JCSS probabilistic model code [73], assuming a normal distribution with a mean of 7850 Kg/m3, a Coefficient of Variation (CoV) of 1.0 %, and using the three-sigma rule of thumb that is equivalent to a confidence interval of 99.7%. For the Young's modulus, the bound values were also set based on a confidence interval of 99.7%, yet, in this case, using a log-normal distribution with a mean of 200 N/mm2 and a CoV of 5%; see [74,75].

As for the thicknesses of the different steel members, the lower bound was defined as the maximum experimental value obtained from the on-site measurements. On the other hand, the upper bound was defined as the initial value (average experimental measurements) minus the maximum theoretical thickness reduction estimated from the current European standards of corrosion in metals [76,77]. According to these standards, as the bridge is located in a coastal area with a significant effect of chlorides, the corrosivity category is C5, implying an annual corrosion rate of 39 μm/year. Thus, given the bridge service life, the maximum theoretical thickness reduction is estimated as 4.65 mm. It is noted that for sensitivity analysis and model updating, uncertainty in thickness dimensions was modeled by means of corrective factors of the base values, i.e., perturbing the average experimental values assuming a uniform variation of the cross-section thicknesses instead of using the many different non-sensitive individual dimensions. Therefore, the adopted parameter bounds aim to define a sufficiently large and reasonable variation range to evaluate the effect of uncertainty in the different cross-section thicknesses of the members on the bridge mass and stiffness and, thus, on the modal properties.

For the stiffness of the rotational and translational springs, the variation ranges were computationally derived from an extensive parametric analysis. Thus, for the rotational springs, the lower and upper bound values represent the threshold for which a pinned or fully rigid behavior is respectively obtained. A similar approach was followed for the translational springs, where the upper bound value represents a scenario of fully constrained displacements, and the lower bound ensures an adequate pairing between numerical and experimental vibration modes with a well-covering of the experimental natural frequencies. In this regard, the adopted mode pairing technique was based on the MAC criterion and the assessment of modal masses to rule out local mode shapes. Table 5 summarizes all the variables with their corresponding lower and upper bounds.

5.2. Surrogate modeling

This work employed surrogate models based on the Kriging approach, which is a statistical interpolation method that allows approximating a scalar-valued FE model response $\hat{y}(\boldsymbol{x})$ for a given vector of input values $\boldsymbol{x} \in \mathbb{R}^m$. The model-building process relies on an experimental design $\boldsymbol{X} = \{\boldsymbol{x}^{(1)}, ..., \boldsymbol{x}^{(N)}\}$ and the associated FE model outcomes $\boldsymbol{Y} = \{y^{(1)}, ..., y^{(N)}\}$, being N the number of training data points. Thus, the approximated functional relationship can be expressed as follows [78]:

$$\hat{y}(\boldsymbol{x}) = \boldsymbol{f}(\boldsymbol{x})^T\boldsymbol{\beta} + Z(\boldsymbol{x}) \tag{6}$$

where the first term $\boldsymbol{f}(\boldsymbol{x})^T\boldsymbol{\beta}$ represents the trend or mean value and consists of P basis functions $\boldsymbol{f}(\boldsymbol{x}) = \left[\boldsymbol{f}_1(\boldsymbol{x}), \cdots, \boldsymbol{f}_p(\boldsymbol{x})\right]^T$ with their corresponding regression coefficients $\boldsymbol{\beta} = \left[\beta_1, \cdots, \beta_p\right]^T$. The second term $Z(\boldsymbol{x})$ is a stationary random process with zero mean and covariance function of the form [79]:

$$Cov(\boldsymbol{x}, \boldsymbol{x}') = \sigma^2 R(\boldsymbol{x}, \boldsymbol{x}'; \theta) \tag{7}$$

where σ^2 denotes the variance, $R(\boldsymbol{x}, \boldsymbol{x}'; \theta)$ represents the correlation function and $\theta = [\theta_1, \cdots, \theta_m]^T$ are hyperparameters obtained by solving an optimization problem, commonly based on a maximum likelihood approach. In this study, in particular, a constant trend (Ordinary Kriging) and an anisotropic Gaussian correlation function were employed, see Equations (8) and (9), [79]:

$$\boldsymbol{f}(\boldsymbol{x})^T\boldsymbol{\beta} = \beta_0 \tag{8}$$

$$R(\boldsymbol{x}, \boldsymbol{x}'; \theta) = \prod_{i=1}^{m} \exp\left[-\frac{1}{2}\left(\frac{|x_i - x_i'|}{\theta_i}\right)^2\right] \tag{9}$$

Surrogate models for each numerical frequency ($\widehat{f}$) and MAC ratio ($\widehat{MAC}$) were trained using a dataset of 1000 sample points. The Design of Experiments (DoE) was generated using the Latin Hypercube Sampling (LHS) method [80]. The prediction accuracy of the surrogate models was quantified based on a 10-fold cross-validation procedure using two different metrics: the coefficient of determination (R^2) and the Root-Mean Square Error (RMSE), Equations (10) and (11), respectively:

$$R^2 = 1 - \frac{\sum_{i=1}^{n}(y_i - \hat{y}_i)^2}{\sum_{i=1}^{n}(y_i - \bar{y})^2} \tag{10}$$

$$RMSE = \sqrt{\frac{1}{n}\sum_{i=1}^{n}(y_i - \hat{y}_i)^2} \tag{11}$$

where y_i denotes the FE model response at the point i, $\hat{y}_i$ is the corresponding surrogate model prediction, $\bar{y}$ is the mean of the response values, and n indicates the total number of samples used in the procedure.

The obtained results are summarized in Table 6. As can be seen, R^2 values equal to or above 0.99 were obtained for all surrogate models. Thus, it can be concluded that the approximation models accurately replicate the outcomes of the more complex and computationally expensive finite element simulations.

Table 5
Parameters considered in the model updating process.

Variable ID	Name	Bounds Lower	Upper
V1	Density (kg/m^3)	7615	8085
V2	Young's modulus (GPa)	170	230
V3	Arch ribs & Tie girders (mm)	1.20	−4.65
V4	Vertical hangers (mm)	1.10	−4.65
V5	Stringers (mm)	1.00	−4.65
V6	Cross-girders (mm)	0.95	−4.65
V7	Reinforcement plates (mm)	1.90	−4.65
V8	Rotational stiffness of steel connections (Nm/rad)	1.00E + 05	1.00E + 08
V9	Z-axis translational stiffness of O Vicedo support (N/m)	1.00E + 05	1.00E + 06
V10	Y-axis translational stiffness of O Vicedo support (N/m)	1.00E + 07	1.00E + 08
V11	Z-axis translational stiffness of O Mañon support (N/m)	1.00E + 05	1.00E + 06
V12	Y-axis translational stiffness of O Mañon support (N/m)	1.00E + 07	1.00E + 08

Table 6
Surrogate modeling results.

Output	R^2	RMSE
$\widehat{f_1}$	0.99	1.50 E-03
$\widehat{f_2}$	0.99	9.70 E-03
$\widehat{f_3}$	0.99	3.10 E-03
$\widehat{f_4}$	0.99	1.43 E-02
$\widehat{MAC}1$	0.99	4.01 E-04
$\widehat{MAC}2$	0.99	8.90 E-03
$\widehat{MAC}3$	0.99	4.89 E-04
$\widehat{MAC}4$	0.99	4.84 E-04

5.3. Sobol' indices

Sobol' indices analyze the sensitivity of each model input by analyzing the model output variance [72]. Thus, the total output variance is expressed as the sum of the partial variances of each input variable and their interaction effects. This variance decomposition allows defining in general terms the sensitivity $S_{i_1,\ldots,i_S}$ as the variance contribution $V_{i_1,\ldots,i_S}$ of a set of variables $\{X_{i_1,\ldots,i_S}\}$ to the total output variance $V(Y)$, [81]:

$$S_{i_1,\ldots,i_S} = \frac{V_{i_1,\ldots,i_S}}{V(Y)} \tag{12}$$

When this formulation is applied to a single input variable, it is called the first-order Sobol' index (S_i), where V_i represents the effect of the variable X_i alone, Equation (13):

$$S_i = \frac{V_i}{V(Y)} \tag{13}$$

Higher-orders Sobol' indices quantify the interaction effects of a group of variables. These interactions cannot be decomposed as contributions of those variables separately. To quantify these interactions, the total Sobol' index (S_{Ti}) is adopted, which is obtained as the sum of the first order (S_i) and higher-orders Sobol' indices ($S_{i,\ i}$), Equation (14):

$$S_{Ti} = S_i + S_{i,\ i} = \frac{V_i + V_{i,\ i}}{V(Y)} \tag{14}$$

where V_i represent the effect of the variable X_i alone, and $V_{i,\ i}$ the interactions effects with all other variables $\boldsymbol{X}_{\ i}$. Thus, this sensitivity measure can be used to identify the non-relevant parameters, i.e., those that can be fixed at any value within the search space without significantly impacting the model output variance.

In this study, the Sobol' sensitivity indices were estimated based on Monte Carlo simulations with the Janon estimator [81,82] using the surrogate models built in the previous section. A threshold value of 5.0 % was established in order to deem a variable as being influential. Thus, Fig. 11 shows the matrix representation of the total sensitivity indices. It can be observed that out of the twelve initial input variables, only seven inputs have a really relevant influence on the natural frequencies and MAC ratios. The most significant are: i) Young's modulus, with a significant effect on the frequencies; ii) the thickness dimensions of the vertical hangers, although minor impacting only the second frequency; iii) the rotational stiffness of the steel connections, similarly to the previous case; and iv) the supports' translational stiffness, with a noticeable impact in the MAC values.

In this regard, the stiffness of the Z-translational springs affects the vibration modes with horizontal displacements (first and second mode), while the Y-translational springs affect the vertical vibration modes (third and fourth mode). As for the rotational springs, it should be noted that, initially, a different variable was assigned to each node in a preliminary stage. However, due to the excessive degree of discretization, these variables were not sensitive for the posterior identification (calibration) process. Therefore, in the final stage, it was decided to group the different parameters according to the damaged state of the connections (see section 3.1. and Fig. 6). In this way, it was possible to enhance identifiability while maintaining physical meaning.

Hence, for the subsequent model updating process, only the seven most influential variables in the bridge modal responses will be considered, while the non-influential inputs will be fixed to their initial value.

6. Optimization approach

The FE model updating process was performed through the minimization of the objective function $\pi(\boldsymbol{x})$:

$$\pi(\boldsymbol{x}) = W_f \sum_{i=1}^{m} \left(\frac{f_{i,num} - f_{i,exp}}{f_{i,exp}} \right)^2 + W_{MAC} \sum_{i=1}^{m} (1 - MAC_i)^2 \tag{15}$$

where $\boldsymbol{x}$ is the vector of calibration parameters, $f_{i,num}$ and $f_{i,exp}$ are the numerical and experimental frequencies of the *i-th* vibration mode, and MAC_i is the corresponding modal assurance criterion between the numerical and experimental mode shapes. m denotes the number of frequencies and mode shapes considered in the updating process, and W_f and W_{MAC} are weighting factors balancing the contribution of each residual term. Herein, weights of 0.75 and 0.25 were adopted since the results of the preliminary (non-calibrated model) FE model already yielded good MAC ratios, being the discrepancies in the natural frequencies higher (see Table 4). Besides, uncertainties associated with the frequencies estimation are generally lower than in the case of the mode shapes [21].

The parameter identification problem was formulated as a nonlinear least-squares problem [83]:

$$min_x \|\pi(\boldsymbol{x})\|_2^2 = min_x \sum_i \pi_i(\boldsymbol{x})^2 \tag{16}$$

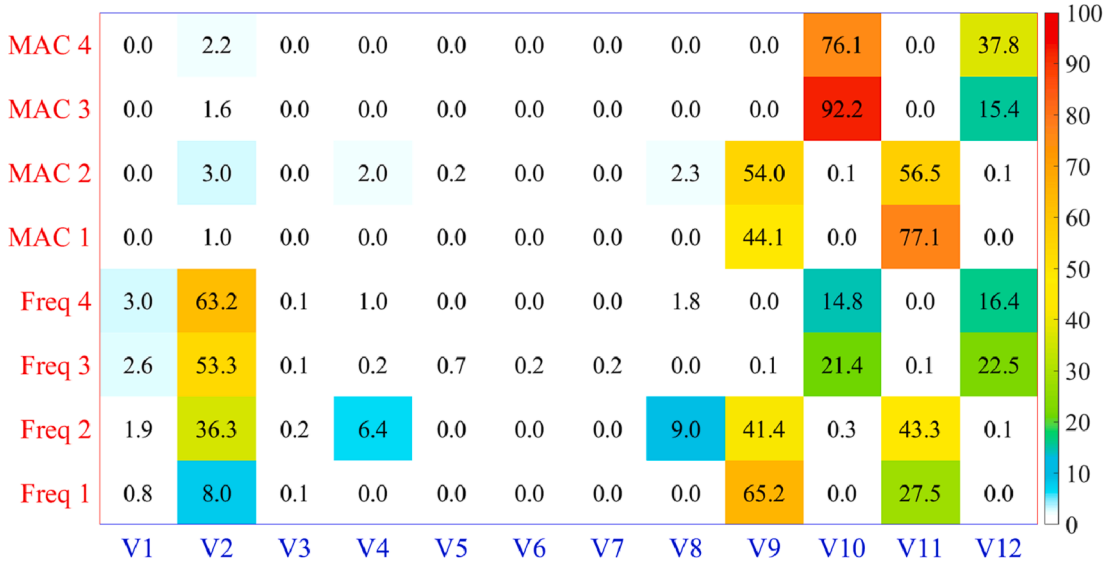

Fig. 11. Matrix of total sensitivity indices (S_{Ti}).

The minimization strategy was implemented through the *lsqnonlin* MATLAB function [83], which is based on a Gauss-Newton method and employs a trust-region-reflective algorithm [84] to solve the optimization problem. This approach determines a trust-region in which a second-order (quadratic) approximation $m(z)$ of the objective function is computed. This approximation is defined by a truncated Taylor series expansion of $\pi(\boldsymbol{x})$ [5]:

$$m(z) = \pi_s + [\nabla \pi_s]^T z + \frac{1}{2} z^T [\nabla^2 \pi_s] z \tag{17}$$

where z is the step vector from $\boldsymbol{x}_s$, the current state vector, and π_s, $\nabla \pi_s$ and $\nabla^2 \pi_s$ are the function value, gradient, and Hessian of π at $\boldsymbol{x}_s$, respectively. The gradient and the Hessian have the following form:

$$\nabla \pi(\boldsymbol{x}) = J_x(\boldsymbol{x})^T \boldsymbol{r}(\boldsymbol{x}) \tag{18}$$

$$\nabla^2 \pi(\boldsymbol{x}) = J_x(\boldsymbol{x})^T J_x(\boldsymbol{x}) + \sum_{i=1}^{k} \boldsymbol{r}_i(\boldsymbol{x}) \nabla^2 \boldsymbol{r}_i(\boldsymbol{x}) \cong J_x(\boldsymbol{x})^T J_x(\boldsymbol{x}) \tag{19}$$

where $\boldsymbol{r}$ is a k-dimensional vector that contains the frequencies and mode shapes residuals, and J is the Jacobian matrix composed of the first partial derivatives of the residuals with respect to the unknown model parameters $\boldsymbol{x}$, which for this application type, are typically calculated by numerical estimates, i.e., by using finite differences.

Since a gradient-based method was adopted, a set of 20 different starting points generated by uniform LHS was considered for performing several independent optimization runs targeted at ensuring a well-covering of the search space, avoiding local minima, and assessing the uniqueness of the identified parameters. Moreover, the objective function in Equation (15) was evaluated for the 1000 FE model runs used as support points in the surrogate modeling process, and the set of parameter entries with the minimum objective function value, i.e., with the lowest sum of the weighted residuals, was also taken as another set of suitable initial values for the optimization algorithm.

The best solution was indeed obtained from the best DoE sample. Nevertheless, similar updated values were also received from various LHS points, underlying the accuracy of the identified model inputs, see Fig. 12. The highest deviations were found in the variables V4, V10, and V12. The variable V4 corresponds with the cross-section thickness dimensions of the vertical hangers, which according to the variance-based sensitivity measures, has only a minor influence on the second eigenfrequency. The variables V10 and V12 are related to the stiffness of the supports in the vertical (Y-axis) direction, which according to the total sensitivity indices, only influences the third and fourth vibration modes, especially the MAC values. Since the MACs of the third and fourth mode shapes are already relatively high for the initial (non-calibrated) model, and the discrepancies in the natural frequencies are, in general, lower than in the first and second vibration modes, both issues, together with the major weighting of the frequency term in the objective function, lead to a lower impact of these variables in the optimization process, which might explain the higher scattering.

Table 7 summarizes the updated parameter values obtained from the best optimization run. The Young's modulus obtained points to an overall deterioration condition due to the aging of the bridge, presenting a reasonable agreement with the estimates from the ultrasonic testing, although slightly lower than the average experimental value. In this regard, it should be noted that this parameter encompasses all structural members, which are affected by different damage effects, such as stress concentration due to corrosion pitting or plates slipping due to lack of rivets, among other issues, which impact the elements' stiffness, and therefore the identified elastic properties. On the other hand, despite the scattering observed given its reduced sensitivity, no significant variations of the thicknesses of the vertical hangers were received with respect to the average experimental measurements, thus indicating a reasonable estimation in the contribution to the overall structural stiffness and mass of the bridge when using this cross-section dimensions. As for the rotational and translational stiffnesses, the calibrated values indicate a semirigid behavior of the steel connections and a nearly symmetrical and slightly asymmetrical response of the bridge supports in the transversal and vertical directions, respectively.

Table 8 reports the relative differences between experimental and numerical frequencies and the MAC values of the calibrated FE model. An average frequency error of 0.34% and an average MAC ratio of 0.96 were obtained, thus denoting a noticeable increase in the correlation between modal properties, especially in the natural frequencies, with a

Table 7
Updated parameter values from the optimization approach.

Variable	Normalized value	Actual value
V2	0.13	178.00 (GPa)
V4	0.37	−1.03 (mm)
V8	0.06	5.69 E + 06 (Nm/rad)
V9	0.38	4.45 E + 05(N/m)
V10	0.75	7.77 E + 07(N/m)
V11	0.42	4.83 E + 05 (N/m)
V12	0.48	5.35 E + 07(N/m)

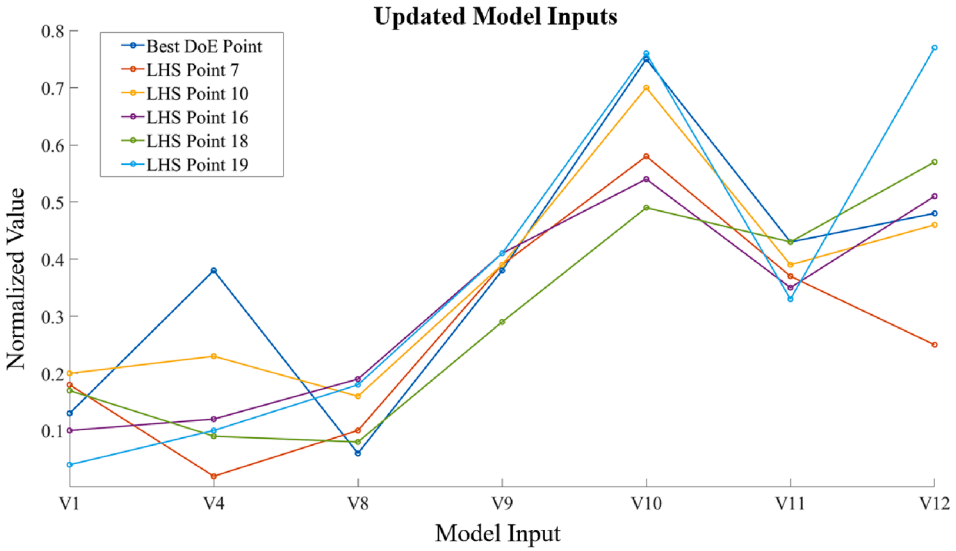

Fig. 12. Updated parameter values for different starting points in the optimization process, normalized between 0 (lower bound) and 1 (upper bound).

discrepancy lower than 1%. Finally, Fig. 13 depicts the numerical mode shapes obtained from the optimization process.

7. Bayesian approach

The Bayesian model updating approach is stated in terms of the following mathematical formulation [85].

$$\boldsymbol{y}^F = \boldsymbol{y}^M(\boldsymbol{x}_M) + \varepsilon(\boldsymbol{x}_\varepsilon) \tag{20}$$

where $\boldsymbol{y}^F$ represents experimental observations of the actual bridge responses, $\boldsymbol{y}^M$ denotes the corresponding FE model outputs for the model inputs ($\boldsymbol{x}_M$), and ε is the so-called discrepancy term, accounting for measurement uncertainties and model inadequacy, i.e., the discrepancy between the best approximations obtained from the numerical model and the actual system behavior [86].

Usually, this error term is modeled as an additive Gaussian discrepancy $\varepsilon\ \mathcal{N}(0, \mathrm{Z})$ with zero mean and covariance matrix of the form $\mathrm{Z} = \sigma^2\boldsymbol{I}$, where $\boldsymbol{I}$ is the identity matrix. Thus, errors are assumed to be independent and identically distributed [87], being the discrepancy function parametrized by $\boldsymbol{x}_\varepsilon = \sigma^2$.

The posterior probability distribution $p(\mathbf{x}|\boldsymbol{y}^F)$ of the uncertain parameters, $\mathbf{x} = (\boldsymbol{x}_M, \boldsymbol{x}_\varepsilon)$, is derived from the application of the Bayes' theorem Equation (21), given the prior probability distribution $p(\mathbf{x})$, and the likelihood of the observations $p(\boldsymbol{y}^F|\mathbf{x})$:

$$p(\mathbf{x}|\boldsymbol{y}^F) \propto p(\boldsymbol{y}^F|\mathbf{x})\, p(\mathbf{x}) \tag{21}$$

The prior probability distribution $p(\mathbf{x})$ represents the initial knowledge about the possible range of values of the parameters before considering the experimental data, and it can be established from a pool of different sources, such as literature data or expert judgment, among others. The likelihood function $p(\boldsymbol{y}^F|\mathbf{x})$, represents the probability of observing the experimental data $\boldsymbol{y}^F$ given particular model and discrepancy parameter values, $\boldsymbol{x}_M$ and $\boldsymbol{x}_\varepsilon$, respectively, and it can be expressed as follows:

$$p(\boldsymbol{y}^F|\boldsymbol{x}_M, \boldsymbol{x}_\varepsilon) = \prod_{i=1}^{N} \mathcal{N}(\boldsymbol{y}^M(\boldsymbol{x}_M), \varepsilon(\boldsymbol{x}_\varepsilon)) \tag{22}$$

where N is the number of independent field observations $\boldsymbol{y}^F = \{\boldsymbol{y}_1, \cdots, \boldsymbol{y}_N\}$, e.g., the modal properties. Thus, the parameter identification problem can be seen as a statistical inference process where the updated distributions $p(\mathbf{x}|\boldsymbol{y}^F)$ of the uncertain parameters are obtained by weighting the prior knowledge with the information contained in the data.

For most complex real-world applications, closed-form expressions for the posterior probability distributions are unavailable. Therefore, simulation techniques such as the Markov Chain Monte Carlo (MCMC) method are employed to draw samples from which to approximate them numerically [88]. The major drawback of MCMC sampling is its high computational cost since it requires a significant number of FE model runs when evaluating the likelihood function. To circumvent this issue, surrogate modeling strategies are introduced, allowing to efficiently and effectively approximate the time-consuming numerical model responses.

In the application of the Bayesian inference framework to the FE model updating of O Barqueiro Bridge, Kriging-based metamodeling, as described in Section 6, was employed in order to mimic the original relationship between the model input parameters $\boldsymbol{x}_M$ and the output (modal) responses $\boldsymbol{y}^M$. Thus, metamodels were built based on a space-filling LHS design of 1000 model runs and using only the seven most influential variables from the sensitivity analysis outcomes. Similarly, R^2 values in the order of 0.99 were obtained in the 10-fold cross-validation process, thus denoting an excellent approximation quality.

In the first stage, named Case-I, non-informative prior uniform distributions with the uncertainty ranges used in the sensitivity analysis procedure were adopted for the model parameters $\boldsymbol{x}_M$. This represents a scenario where only a limited knowledge of the model input values is available. Thus, a conservative assumption is made, expecting that the posterior distributions are dominated by the likelihood function, i.e., the information contained in the experimental data. For the discrepancy variance σ^2, a similar approach as in [89] was followed, assuming a uniform distribution with the lower bound equal to zero and the upper bound given by the average error in frequencies obtained at exercising the surrogate models for the calibrated values yielded from optimization. As for the field observations, given the relatively high MAC coefficients already received from the uncalibrated model and the higher relevance of the frequency term in the inverse identification of model parameters as revealed from the deterministic approach, only the experimental frequencies were used in the likelihood function evaluation. Finally, samples from the posterior distribution of the uncertain parameters were drawn using the MCMC method with the affine invariant ensemble sampler (AIES) algorithm [90,91] for a total of 30,000 simulations and a half burn-in phase in order to obtain unbiased estimates.

The posterior distributions are shown in Fig. 14, with the mean and standard deviation provided in Table 9. According to the global variance-based sensitivity analysis results, and taking the empirical mean values as the point estimate, it can be observed that a good agreement with respect to the optimized values was found for the most influential variables (V2, V9, V10, V11, V12), especially for those major impacting the first and second natural frequencies (V2, V9, and V11). This agrees with the observations from the optimization-based model updating process; see Fig. 12 and related discussion. On the contrary, the highest discrepancies were found in the variables V4 and V8, given their lower sensitivity, as they are only relevant in the second eigenfrequency. This makes identifiability more difficult, as denoted by the higher scattering compared to the most influential variables, where the standard deviation is significantly lower. Table 11 reports the natural frequencies and MAC values obtained by re-running the original FE model at the posterior mean estimates. Accordingly, the results indicate an average relative error in frequencies of 0.58% and an average MAC value of 0.95 for the updated FE model. It is worth noting that evaluating the metamodels at the same input values, a maximum local approximation error of 0.16% was observed at the second eigenfrequency, thus highlighting the usefulness and reliability of the surrogate modeling process for the efficient solution of the inverse problem.

In the second stage (Case-II)), aiming to evaluate the impact of the prior distributions on the calibration results, weakly informative prior distributions were used for the model parameters in the form of triangular probability distributions. Thus, as in the deterministic approach, the best design obtained in the sensitivity analysis was used as the mode

Table 8
Modal properties after optimization-based model updating.

Mode	Experimental f_{exp}(Hz)	Updated model f_{num}(Hz)	Error (%)	MAC
1	1.051	1.052	0.08%	0.99
2	2.713	2.706	0.27%	0.92
3	6.190	6.186	0.06%	0.95
4	7.363	7.296	0.91%	0.98

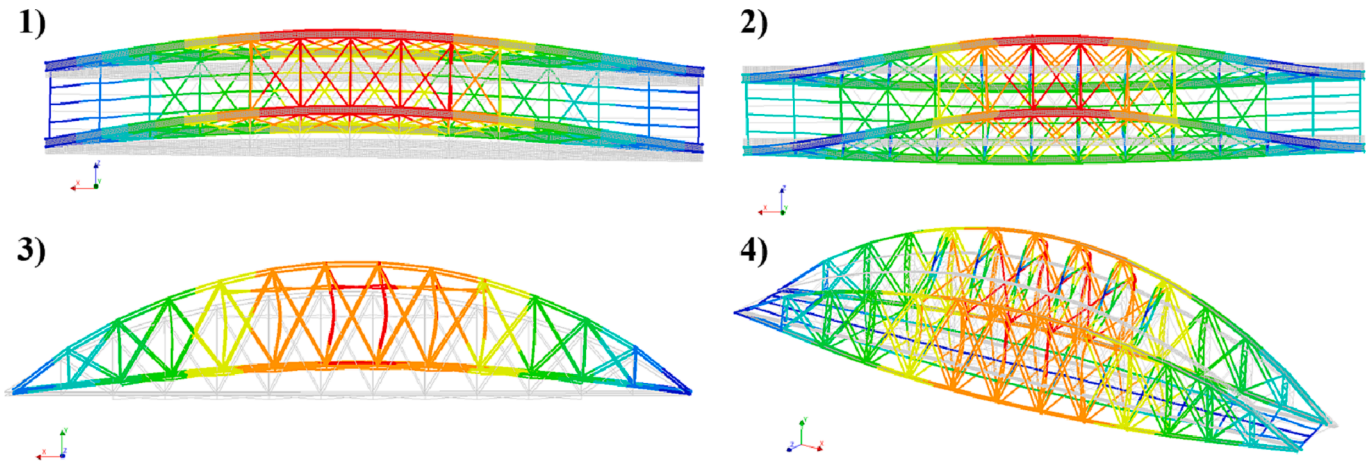

Fig. 13. Mode shapes after optimization-based model updating.

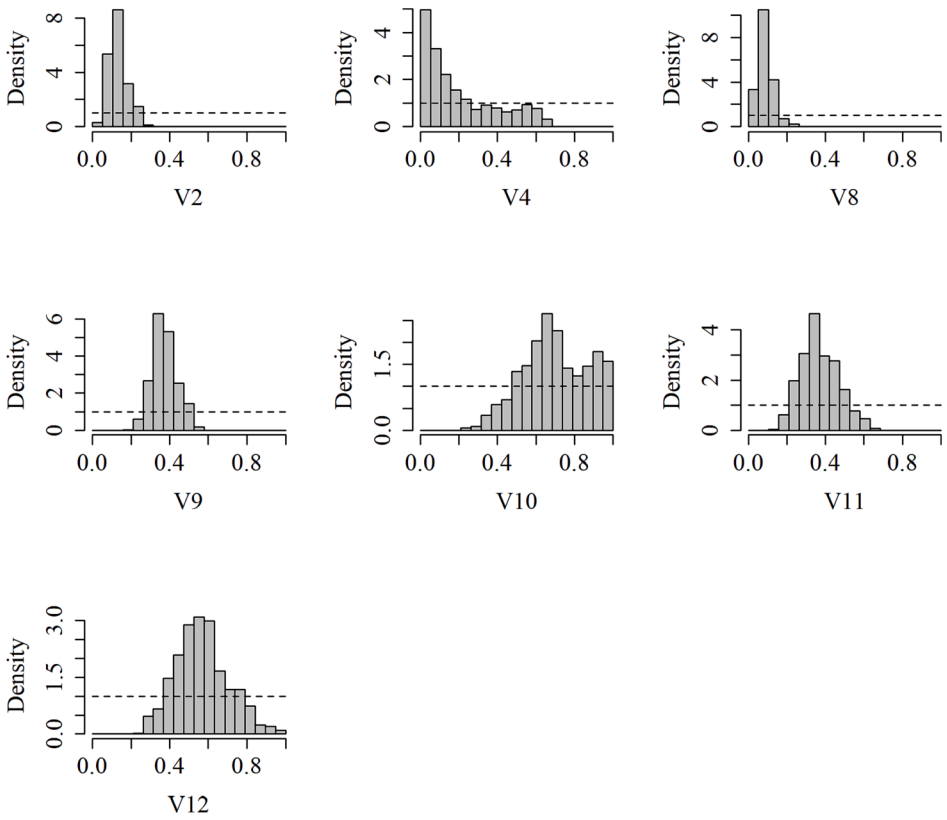

Fig. 14. Posterior probability distributions of the uncertain model parameters from Bayesian calibration when using uniform prior distributions.

Table 9
Mean and standard deviation of the posterior distributions of the uncertain model parameters after Bayesian calibration using uniform prior distributions.

Variable	Normalized value		Actual value	
	Mean	Standard deviation	Mean	Standard deviation
V2	0.13	0.05	178.00 GPa	3.00 GPa
V4	0.21	0.19	−0.12 mm	1.09 mm
V8	0.09	0.04	9.10 E + 06 (Nm/rad)	4.00 E + 06 (Nm/rad)
V9	0.37	0.06	4.33 E + 05 (N/m)	5.40 E + 04 (N/m)
V10	0.70	0.17	7.30 E + 07 (N/m)	1.53 E + 07 (N/m)
V11	0.37	0.10	4.33 E + 05 (N/m)	9.00 E + 04 (N/m)
V12	0.57	0.14	6.13 E + 07 (N/m)	1.26 E + 07 (N/m)

value of the distributions together with the lower and upper bounds corresponding to the uncertainty ranges of Table 5. By drawing samples using the MCMC method, the obtained posterior distributions are shown in Fig. 15, with the mean and standard deviation indicated in Table 10. In general, the posterior means show similar values as in the previous case; however, a general trend regarding uncertainty reduction can be noticed, especially for the less influential model inputs. This fact suggests that identifiability can be improved if reasonable initial information regarding the most likely parameter values is available, which is especially useful in the case of the less influential variables as the information contained in the experimental data is enriched with this prior knowledge, thus making the identification process more effective. Moreover, the overall agreement between the calibrated parameter values using both deterministic and probabilistic approaches was also

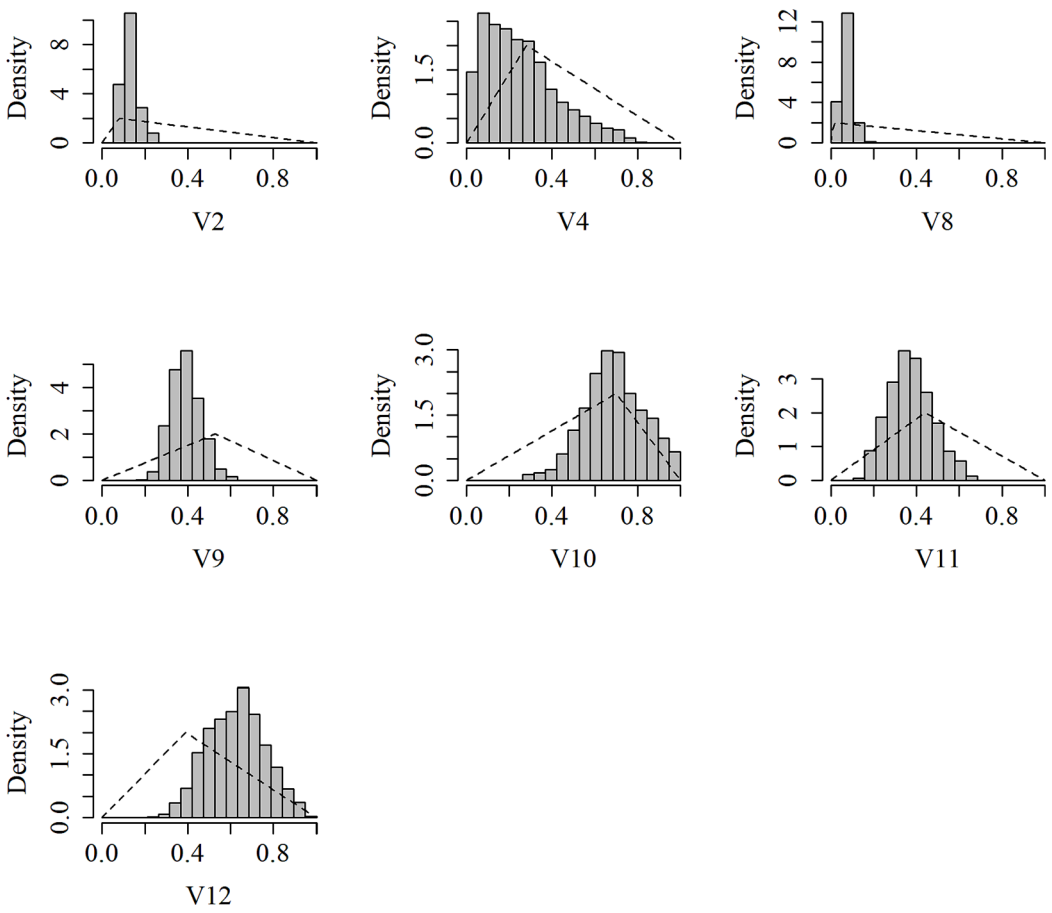

Fig. 15. Posterior probability distributions of the uncertain model parameters from Bayesian calibration when using triangular prior distributions.

Table 10
Mean and standard deviation of the posterior distributions of the uncertain model parameters after Bayesian calibration using triangular prior distributions.

Variable	Normalized value		Actual value	
	Mean	Standard deviation	Mean	Standard deviation
V2	0.13	0.04	178.00 GPa	2.40 GPa
V4	0.25	0.17	−0.34 mm	0.98 mm
V8	0.07	0.03	7.10 E + 06 (Nm/rad)	3.00 E + 06 (Nm/rad)
V9	0.39	0.07	4.51 E + 05 (N/m)	6.30 E + 04 (N/m)
V10	0.69	0.14	7.21 E + 07 (N/m)	1.26 E + 07 (N/m)
V11	0.37	0.10	4.33 E + 05 (N/m)	9.00 E + 04 (N/m)
V12	0.62	0.13	6.58 E + 07 (N/m)	1.17 E + 07 (N/m)

improved. Thus, using the posterior mean estimates, the updated FE model showed an average relative error in frequencies of 0.44% and an average MAC value of 0.95, see Table 11.

The close match between the parameter values received from the different starting points in the optimization process and the noticeable agreement with the probabilistic Bayesian estimate corroborates the robustness of the FE model updating results. Nonetheless, the attractiveness of the Bayesian framework is underlined since, in addition to the advantage of explicitly taking into account possible measurement errors or model inadequacy, it further provides a full posterior probability distribution of the uncertain parameters rather than a pointwise estimation, as it the case in single-objective optimization strategies. This means that many other feasible solutions to the parameter identification problem with high likelihood values are retained and that these distributions can be further exploited to derive probabilistic predictions of the output responses of interest. Accordingly, in Fig. 16, the posterior predictive distributions of the numerical frequencies obtained from Case-II using 1000 sampling points are given together with the experimental data and the FE model results at the optimal parameter set from the deterministic approach; it can be appreciated that the range of the posterior predictions successfully covers the experimental frequencies.

Table 11
Modal properties after Bayesian model updating.

Mode	Experimental	Uniform priors			Triangular priors		
	f_{exp}(Hz)	f_{num}(Hz)	Error %	MAC	f_{num}(Hz)	Error %	MAC
1	1.051	1.047	0.40	0.99	1.051	0.02	0.99
2	2.713	2.756	1.57	0.91	2.747	1.24	0.91
3	6.190	6.210	0.32	0.93	6.215	0.41	0.93
4	7.363	7.360	0.04	0.98	7.356	0.09	0.98

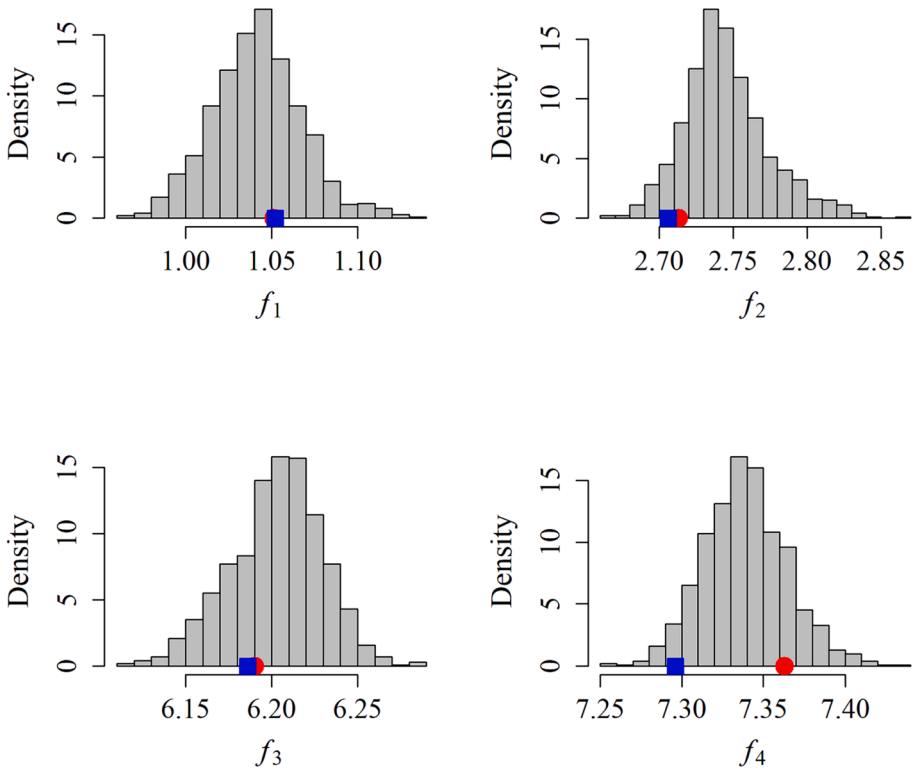

Fig. 16. Posterior predictive distributions (histograms) for the natural frequencies, experimental data (red circle), and estimations from the optimization-based calibration approach (blue square). (For interpretation of the references to colour in this figure legend, the reader is referred to the web version of this article.)

8. Conclusions

This work proposed a methodology for FE model updating of aging steel bridges based on deterministic and probabilistic approaches. The in-practice implementation feasibility has been evaluated in a riveted steel bridge in Galicia, Spain. Due to its damaged condition and aging, the structure represents a fairly challenging case study. The proposed methodology encompasses several stages ranging from a multidisciplinary in-situ non-destructive experimental characterization to the FEM-based numerical modeling and subsequent calibration. The main conclusions that can be drawn from the study are outlined in the following:

- Aging bridges are typically subjected to adverse environmental effects that lead to the decay and degradation of their steel members and connections, thus causing the experimental characterization to be a rather complex procedure. The problem is further compounded in the case of heritage constructions, as additional constraints arise when performing the experimental tests, given the need to preserve the appearance and integrity of the construction. Therefore, NDT techniques have been postulated as the preferable solution. Accordingly, in this application, it was shown how the combined use of different NDT surveying methods could be an effective practical approach. Thus, LIDAR point cloud data and on-site manual measurements can be synergistically used for overall and local geometrical characterization when design drawings do not exist or do not adequately represent the current construction aspect. Ultrasonic testing might be employed to get initial estimates of steel elastic properties, namely Young's modulus. Finally, full-scale ambient vibration testing allows for assessing the structural dynamic behavior and provides the ground truth data (modal properties) for the FE model updating process.
- Sensitivity analysis plays a crucial role in the calibration process. It helps to better understand the underlying bridge mechanics and filter non-influential variables that otherwise could not be identified in the FE model updating process, resulting in improved accuracy and efficiency (due to dimensionality reduction). In this application, a global variance-based sensitivity analysis methodology combined with a Kriging surrogate modeling strategy was adopted. Thus, from a set of 1000 model runs, accurate surrogate models were trained, and Sobol' indices were derived, allowing the discarding of six out of the initial thirteen uncertain parameters for the subsequent calibration procedure.
- The information obtained from exploring the search space in the design of experiments conducted for the surrogate model building can be further exploited to select suitable parameter values as starting points in the optimization algorithm and to define possible prior distributions in the Bayesian inference process. Accordingly, in this application, this enabled delivering the best set of calibrated values from optimization as well as reducing parameter uncertainties in the Bayesian inference approach, especially for the less influential model inputs.
- When using local optimization methods, such as gradient-based, it is of utmost importance to perform several optimization runs from different starting points. This process is highly valuable to avoid local minima and analyze the accuracy and stability of the identified parameter values. Accordingly, in this application, a dataset of 21 different starting points was employed, showing the corresponding optimization results a very good agreement among the updated values for the most sensitive variables and a slightly higher scattering for the less influential ones.
- Bayesian inference is an appealing approach for FE model updating of aging bridges as an alternative to the most widespread optimization-based deterministic approaches. It explicitly considers measurement errors and model inadequacy and allows uncertainty quantification regarding model input parameters, which can be further exploited to derive probabilistic measures of the outputs of interest. In this application, two different assumptions regarding the

prior distribution of the uncertain parameters were considered to evaluate the impact on the updated posterior distributions. Accordingly, the first assumed non-informative (uniform) distributions, while the second case used weakly informative (triangular) prior distributions. The results yielded similar estimates for the posterior means but with a general trend towards uncertainty reduction in the second case. A good agreement was also found with the results from deterministic calibration, thus highlighting the robustness of the FE model updating process.

This work aims to contribute to the development of robust methodologies where uncertainty quantification is carried through all stages of the FE model updating process, especially with respect to aging steel bridges. Future research lines may explore using processing techniques that allow for probabilistically analyzing the vibration-based data. Other lines of action might also explore incorporating the effect of environmental conditions, such as temperature or wind, that modify the dynamic response of the structure. This could be accomplished using continuous monitoring so as to derive a probabilistic description of the experimental natural frequencies, which can then be incorporated into the calibration process through, e.g., Bayesian inference.

CRediT authorship contribution statement

B. Barros: Methodology, Software, Investigation, Writing – original draft. **B. Conde:** Conceptualization, Methodology, Investigation, Supervision, Writing – review & editing. **M. Cabaleiro:** Investigation, Resources, Supervision. **B. Riveiro:** Funding acquisition, Supervision, Writing – review & editing.

Declaration of Competing Interest

The authors declare that they have no known competing financial interests or personal relationships that could have appeared to influence the work reported in this paper.

Acknowledgments

This work has received funding from the European Union's Horizon 2020 research and innovation program under grant agreement No. 958171. Work produced with the support of a 2021 Leonardo Grant for Researchers and Cultural Creators, BBVA Foundation. The BBVA Foundation takes no responsibility for the opinions, statements, and contents of this project, which are entirely the responsibility of its authors. This work has been partially supported by the Spanish Ministry of Science, Innovation, and Universities through the grant PRE2019-087331.

References

[1] González-Jorge H, Gonzalez-Aguilera D, Rodriguez-Gonzalvez P, Arias P. Monitoring biological crusts in civil engineering structures using intensity data from terrestrial laser scanners. Constr Build Mater 2012;31:119–28. https://doi.org/10.1016/j.conbuildmat.2011.12.053.
[2] de Ville de Goyet V. Arch Bridges or Bridges with Arches, Elegant and Efficient Solutions to Cross an Obstacle. Proceedings of Arch; 2019. https://doi.org/10.1007/978-3-030-29227-0_3.
[3] J. Jensen, *History of Bridges-A philatelic review*. 2001.
[4] "Report card for america's infraestructure," pp. 18–25, [Online]. Available: https://infrastructurereportcard.org/cat-item/bridges-infrastructure/.
[5] Teughels A, Maeck J, De Roeck G. Damage assessment by FE model updating using damage functions. Comput Struct 2002;80(25):1869–79. https://doi.org/10.1016/S0045-7949(02)00217-1.
[6] Hou R, Xia Y. Review on the new development of vibration-based damage identification for civil engineering structures: 2010–2019. J Sound Vib 2021;491:115741. https://doi.org/10.1016/j.jsv.2020.115741.
[7] Ye C, Kuok S-C, Butler LJ, Middleton CR. Implementing bridge model updating for operation and maintenance purposes: examination based on UK practitioners' views. Struct Infrastruct Eng 2022;18(12):1638–57.
[8] Gunnstein OØ, Frøseth T, Rönnquist Anders. Operational modal analysis and model updating of Riveted steel bridge. Conf Proc Soc Exp Mech Ser 2016;2:229–35. https://doi.org/10.1007/978-3-319-29751-4_23.
[9] Zordan T, Briseghella B, Liu T. Finite element model updating of a tied-arch bridge using Douglas-Reid method and Rosenbrock optimization algorithm. J Traffic Transp Eng (English Ed 2014;1(4):280–92. https://doi.org/10.1016/S2095-7564(15)30273-7.
[10] Ereiz S, Duvnjak I, Fernando Jiménez-Alonso J. Review of finite element model updating methods for structural applications. Structures 2022;41(April):684–723. https://doi.org/10.1016/j.istruc.2022.05.041.
[11] El Masri Y, Rakha T. A scoping review of non-destructive testing (NDT) techniques in building performance diagnostic inspections. Constr Build Mater 2020;265:120542. https://doi.org/10.1016/j.conbuildmat.2020.120542.
[12] Kashif Ur Rehman S, Ibrahim Z, Memon SA, Jameel M. Nondestructive test methods for concrete bridges: A review. Constr Build Mater 2016. https://doi.org/10.1016/j.conbuildmat.2015.12.011107.
[13] Pallarés FJ, Betti M, Bartoli G, Pallarés L. Structural health monitoring (SHM) and Nondestructive testing (NDT) of slender masonry structures: A practical review. Constr Build Mater 2021. https://doi.org/10.1016/j.conbuildmat.2015.12.011.
[14] Lim MK, Cao H. Combining multiple NDT methods to improve testing effectiveness. Constr Build Mater 2013;38:1310–5. https://doi.org/10.1016/j.conbuildmat.2011.01.011.
[15] Sánchez-Aparicio LJ, Riveiro B, González-Aguilera D, Ramos LF. The combination of geomatic approaches and operational modal analysis to improve calibration of finite element models: A case of study in Saint Torcato Church (Guimarães, Portugal). Constr Build Mater 2014;70:118–29. https://doi.org/10.1016/j.conbuildmat.2014.07.106.
[16] Zárate BA, Caicedo JM. Finite element model updating: Multiple alternatives. Eng Struct 2008;30(12):3724–30. https://doi.org/10.1016/j.engstruct.2008.06.012.
[17] J. C. Matos, V. N. Moreira, I. B. Valente, P. J. S. Cruz, L. C. Neves, and N. Galvão, "Probabilistic-based assessment of existing steel-concrete composite bridges – Application to Sousa River Bridge," *Eng. Struct.*, vol. 181, no. December 2018, pp. 95–110, 2019, doi: 10.1016/j.engstruct.2018.12.006.
[18] Moropoulou A, Labropoulos KC, Delegou ET, Karoglou M, Bakolas A. Non-destructive techniques as a tool for the protection of built cultural heritage. Constr Build Mater 2013;48:1222–39. https://doi.org/10.1016/j.conbuildmat.2013.03.044.
[19] Adam JM, Bett M, Clementi F, Ivorra S. Structural health monitoring and NDT of masonry structures: Research and practice. Constr. Build. Mater. 2022;314(November 2021):125704. https://doi.org/10.1016/j.conbuildmat.2021.125704.
[20] Bautista-De Castro Á, Sánchez-Aparicio LJ, Carrasco-García P, Ramos LF, González-Aguilera D. A multidisciplinary approach to calibrating advanced numerical simulations of masonry arch bridges. Mech Syst Signal Process 2019;129:337–65. https://doi.org/10.1016/j.ymssp.2019.04.043.
[21] Conde B, Ramos LF, Oliveira DV, Riveiro B, Solla M. Structural assessment of masonry arch bridges by combination of non-destructive testing techniques and three-dimensional numerical modelling: Application to Vilanova bridge. Eng Struct 2017;148:621–38. https://doi.org/10.1016/j.engstruct.2017.07.011.
[22] Pepi C, Cavalagli N, Gusella V, Gioffr M. An integrated approach for the numerical modeling of severely damaged historic structures : Application to a masonry bridge. Adv Eng Softw 2020;151(January):2021. https://doi.org/10.1016/j.advengsoft.2020.102935.
[23] Costa BJA, Magalhães F, Cunha Á, Figueiras J. Rehabilitation assessment of a centenary steel bridge based on modal analysis. Eng Struct 2013;56:260–72. https://doi.org/10.1016/j.engstruct.2013.05.010.
[24] Ribeiro D, Calçada R, Delgado R, Brehm M, Zabel V. Finite element model updating of a bowstring-arch railway bridge based on experimental modal parameters. Eng Struct 2012;40:413–35. https://doi.org/10.1016/j.engstruct.2012.03.013.
[25] H. Tran-Ngoc, S. Khatir, G. De Roeck, T. Bui-Tien, L. Nguyen-Ngoc, and M. Abdel Wahab, "Model updating for nam O bridge using particle swarm optimization algorithm and genetic algorithm," *Sensors (Switzerland)*, vol. 18, no. 12, 2018, doi: 10.3390/s18124131.
[26] Sánchez-Aparicio LJ, Bautista-De Castro Á, Conde B, Carrasco P, Ramos LF. Non-destructive means and methods for structural diagnosis of masonry arch bridges. Autom Constr 2019;104(May):360–82. https://doi.org/10.1016/j.autcon.2019.04.021.
[27] Carvalho J, Datta BN, Gupta A, Lagadapati M. A direct method for model updating with incomplete measured data and without spurious modes. Mech Syst Signal Process 2007;21(7):2715–31. https://doi.org/10.1016/j.ymssp.2007.03.001.
[28] Yang YB, Chen YJ. A new direct method for updating structural models based on measured modal data. Eng Struct 2009;31(1):32–42. https://doi.org/10.1016/j.engstruct.2008.07.011.
[29] Deng L, Asce AM, Cai CS, Asce F. Bridge Model Updating Using Response Surface Method and Genetic Algorithm. J Bridg Eng 2010;no. October:553–64. https://doi.org/10.1061/(ASCE)BE.1943-5592.0000092.
[30] Jiménez-Alonso JF, Naranjo-Perez J, Pavic A, Sáez A. Maximum Likelihood Finite-Element Model Updating of Civil Engineering Structures Using Nature-Inspired Computational Algorithms. Struct Eng Int 2021;(3):326–38. https://doi.org/10.1080/10168664.2020.1768812.
[31] Hofmeister B, Bruns M, Rolfes R. Finite element model updating using deterministic optimisation : A global pattern search approach. Eng Struct 2019;195(May):373–81. https://doi.org/10.1016/j.engstruct.2019.05.047.
[32] Tran-Ngoc H, Khatir S, Le-Xuan T, De Roeck G, Bui-Tien T, Abdel Wahab M. Finite element model updating of a multispan bridge with a hybrid metaheuristic search algorithm using experimental data from wireless triaxial sensors. Eng Comput 2022;38(s3):1865–83. https://doi.org/10.1007/s00366-021-01307-9.
[33] Naranjo-Pérez J, Jiménez-Alonso JF, Pavic A, Sáez A. Finite-element-model updating of civil engineering structures using a hybrid UKF-HS algorithm. Struct

Infrastruct Eng 2021;17(5):620–37. https://doi.org/10.1080/15732479.2020.1760317.
[34] Bouzas O, Conde B, Cabaleiro M, Riveiro B. A holistic methodology for the non-destructive experimental characterization and reliability-based structural assessment of historical steel bridges. Eng Struct 2022;vol. 270, no. May:114867. https://doi.org/10.1016/j.engstruct.2022.114867.
[35] Jesus A, Brommer P, Zhu Y, Laory I. Comprehensive Bayesian structural identification using temperature variation. Eng Struct 2017;141:75–82. https://doi.org/10.1016/j.engstruct.2017.01.060.
[36] Pepi C, Gioffrè M, Grigoriu M. Bayesian inference for parameters estimation using experimental data. Probabilistic Eng Mech 2020;60(January). https://doi.org/10.1016/j.probengmech.2020.103025.
[37] Mao J, Wang H, Li J. Bayesian Finite Element Model Updating of a Long-Span Suspension Bridge Utilizing Hybrid Monte Carlo Simulation and Kriging Predictor. KSCE J Civ Eng 2020. https://doi.org/10.1007/s12205-020-0983-4.
[38] Baisthakur S, Chakraborty A. Modified Hamiltonian Monte Carlo-based Bayesian finite element model updating of steel truss bridge. Struct Control Heal Monit 2020;27(8):1–22. https://doi.org/10.1002/stc.2556.
[39] Boulkaibet I, Mthembu L, Marwala T, Friswell MI, Adhikari S. Finite element model updating using Hamiltonian Monte Carlo techniques. Inverse Probl Sci Eng 2017;25(7):1042–70. https://doi.org/10.1080/17415977.2016.1215446.
[40] Argyris C, Papadimitriou C, Panetsos P, Tsopelas P. Bayesian Model-Updating Using Features of Modal Data : Application to the Metsovo Bridge. Sens Actuator Networks 2020. https://doi.org/10.3390/jsan9020027.
[41] J. Ching and Y. Chen, "Transitional Markov Chain Monte Carlo Method for Bayesian Model Updating, Model Class Selection, and Model Averaging," 2007, doi: 10.1061/(ASCE)0733-9399(2007)133:7(816).
[42] Cheung SH, Bansal S. A new Gibbs sampling-based algorithm for Bayesian model updating with incomplete complex modal data. Mech Syst Signal Process 2017;92:156–72. https://doi.org/10.1016/j.ymssp.2017.01.015.
[43] Yuen KV, Ortiz GA. Multiresolution Bayesian nonparametric general regression for structural model updating. Struct Control Heal Monit 2018;25(2):1–14. https://doi.org/10.1002/stc.2077.
[44] Marin JM, Pudlo P, Robert CP, Ryder RJ. Approximate Bayesian computational methods. Stat Comput 2012;22(6):1167–80. https://doi.org/10.1007/s11222-011-9288-2.
[45] Vakilzadeh MK, Huang Y, Beck JL, Abrahamsson T. Approximate Bayesian Computation by Subset Simulation using hierarchical state-space models. Mech Syst Signal Process 2017;84:2–20. https://doi.org/10.1016/j.ymssp.2016.02.024.
[46] Bishop CM. Pattern Recognition and Machine Learning, vol. 23, no. 6. Springer; 2006.
[47] Li B, Der Kiureghian A. Operational modal identification using variational Bayes. Mech Syst Signal. Process 2017;88:377–98. https://doi.org/10.1016/j.ymssp.2016.11.007.
[48] Huang Y, Shao C, Wu B, Beck JL, Li H. State-of-the-art review on Bayesian inference in structural system identification and damage assessment. Adv Struct Eng 2019;22(6):1329–51. https://doi.org/10.1177/1369433218811540.
[49] Simoen E, De Roeck G, Lombaert G. Dealing with uncertainty in model updating for damage assessment: A review. Mech Syst Signal Process 2015;56:123–49. https://doi.org/10.1016/j.ymssp.2014.11.001.
[50] Akhlaghi MM, Bose S, Mohammadi ME, Moaveni B, Stavridis A, Wood RL. Post-earthquake damage identification of an RC school building in Nepal using ambient vibration and point cloud data. Eng Struct 2021. https://doi.org/10.1016/j.engstruct.2020.111413.
[51] Ponsi F, Bassoli E, Vincenzi L. Bayesian and deterministic surrogate-assisted approaches for model updating of historical masonry towers. J Civ Struct Heal Monit 2022. https://doi.org/10.1007/s13349-022-00594-0.
[52] A. De Falco, M. Girardi, D. Pellegrini, L. Robol, and G. Sevieri, "Model parameter estimation using Bayesian and deterministic approaches : case study of the Maddalena Bridge," *XIV Int. Conf. Build. Pathol. Constr. Repair* –, vol. 11, pp. 210–217, 2018, doi: 10.1016/j.prostr.2018.11.028.
[53] Behmanesh I, Moaveni B. Probabilistic identification of simulated damage on the Dowling Hall footbridge through Bayesian finite element model updating. Struct. Control Heal. Monit. 2015;(August 2014):463–83. https://doi.org/10.1002/stc.1684.
[54] S. A. Blanco, M. D. Fuentes, and C. N. Ortiz, *Pontes históricas de Galicia.* 1991.
[55] Valença J, Puente I, Júlio E, González-Jorge H, Arias-Sánchez P. Assessment of cracks on concrete bridges using image processing supported by laser scanning survey. Constr Build Mater 2017;146:668–78. https://doi.org/10.1016/j.conbuildmat.2017.04.096.
[56] Riveiro B, Morer P, Arias P, De Arteaga I. Terrestrial laser scanning and limit analysis of masonry arch bridges. Constr Build Mater 2011;25(4):1726–35. https://doi.org/10.1016/j.conbuildmat.2010.11.094.
[57] Conde B, Díaz-Vilariño L, Lagüela S, Arias P. Structural analysis of Monforte de Lemos masonry arch bridge considering the influence of the geometry of the arches and fill material on the collapse load estimation. Constr Build Mater 2016;120:630–42. https://doi.org/10.1016/j.conbuildmat.2016.05.107.
[58] "Faro Focus 3 D (FARO Technologies Inc., Lake Mary, Florida, USA)." https://www.faro.com/.
[59] Krautkrämer J, Krautkrämer H, Sachse W. Ultrasonic Testing of Materials. Berlin Heidelberg: Springer-Vedag; 1990.
[60] "MX-3 Dakota Ultrasonics," *1500 Green Hills Road, Scotts Valley, California, EEUU*. https://dakotaultrasonics.com/.
[61] Brincker R, Ventura CE. Introduction to operational modal analysis. John Wiley & Sons Ltd; 2015.
[62] da JLF, Ramos S. Damage Identification on Masonry Structures Based on Vibration Signatures Identificação de Dano em Estruturas de Alvenaria Baseada na Medição de Vibrações. Universidade do Minho 2007.
[63] J. Rodrigues, "Identificação Modal Estocástica: Métodos de Análise e Aplicações em Estruturas de Engenharia Civil," 2004.
[64] "BRÜEL & KJAER and HBK company." https://www.bksv.com/.
[65] "Artemis Modal." Aalborg East Denmark, 1999, [Online]. Available: https://svibs.com/artemis-modal/.
[66] Brincker R, Ventura CE, Andersen P. Damping Estimation by Frequency Domain Decomposition. IMAC 2001;19.
[67] Brincker R, Andersen P. Understanding Stochastic Subspace Identification. Conf. Proc. Soc. Exp. Mech Ser. 2006.
[68] H. Shokravi and N. H. Bakhary, "Comparative analysis of different weight matrices in subspace system identification for structural health monitoring," *IOP Conf. Ser. Mater. Sci. Eng.*, vol. 271, no. 1, 2017, doi: 10.1088/1757-899X/271/1/012092.
[69] Computational Mechanics Department of TNO Building and construction research institute, "DIANA FEA BV Documentation." Delft, The Netherlands, 2003, [Online]. Available: https://dianafea.com.
[70] "MATLAB." The MathWorks Inc, Natick, Massachusetts:, [Online]. Available: https://es.mathworks.com/products/matlab.html.
[71] Park YS, Kim S, Kim N, Lee JJ. Finite element model updating considering boundary conditions using neural networks. Eng Struct 2017;150:511–9. https://doi.org/10.1016/j.engstruct.2017.07.032.
[72] Sobol IM. Global sensitivity indices for nonlinear mathematical models and their Monte Carlo estimates. Math Comput Simul 2001;55(1–3):271–80. https://doi.org/10.1016/S0378-4754(00)00270-6.
[73] JCSS, "Probabilistic Model Code - Part 2: Load Models," pp. 1–73, 2001, [Online]. Available: https://www.jcss-lc.org/publications/jcsspmc/part_ii.pdf.
[74] Barbato M, Gu Q, Conte JP. Probabilistic Push-Over Analysis of Structural and Soil-Structure Systems. J Struct Eng 2010. https://doi.org/10.1061/(ASCE)ST.1943-541X.0000231.
[75] Park CB, Miller RD, Xia J. Multichannel analysis of surface waves. Geophysics 1999;64:800–8. https://doi.org/10.1190/1.1444590.
[76] *AENOR Part 1: Corrosion of metals and alloys - Corrosivity of atmospheres - Classification, determination and estimation (ISO 92232012)*.
[77] *AENOR Part 2:Corrosion of metals and alloys - Corrosivity of atmospheres - Guiding values for the corrosivity categories (ISO 9224:2012)*.
[78] Sacks J, Welch WJ, Mitchell YJ, Wynn HP. Design and Analysis of Computer Experiments. Stat Sci 1989;4:409–35. https://doi.org/10.1214/ss/1177012413.
[79] C. Lataniotis, S. Marelli, and B. Sudret, "Kriging UqLab User Manual (Gaussian Process Modelling)," [Online]. Available: https://www.uqlab.com/user-manuals.
[80] McKay MD, Beckman RJ, Conover WJ. Comparison of three methods for selecting values of input variables in the analysis of output from a computer code. Technometrics 1979;21(2):239–45. https://doi.org/10.1080/00401706.1979.10489755.
[81] S. Marelli C. Lamas K. Konakli C. Mylonas P. Wiederkehr B. Sudret, "UQLab User Manual (Sensitivity Analysis)," [Online]. Available: https://www.uqlab.com/sensitivity-user-manual.
[82] Janon A, Klein T, Lagnoux A, Nodet M, Prieur C. Asymptotic normality and efficiency of two Sobol index estimators. ESAIM - Probab Stat 2014;18:342–64. https://doi.org/10.1051/ps/2013040.
[83] Mathworks, "MathWorks. MatLab user manual,Least-Squares (Model Fitting) Algorithms." https://es.mathworks.com/help/optim/ug/least-squares-model-fitting-algorithms.html.
[84] Coleman TF, Li Y. An interior trust region approach for nonlinear minimization subject to bounds. SIAM J Optim 1996;6(2):418–45. https://doi.org/10.1137/0806023.
[85] Wagner P-R, Fahrni R, Klippel M, Frangi A, Sudret B. Bayesian calibration and sensitivity analysis of heat transfer models for fire insulation panels. Eng Struct 2020. https://doi.org/10.1016/j.engstruct.2019.110063.
[86] Conde B, Eguía P, Stavroulakis GE, Granada E. Parameter identification for damaged condition investigation on masonry arch bridges using a Bayesian approach. Eng Struct 2018;172(June):275–84. https://doi.org/10.1016/j.engstruct.2018.06.040.
[87] Conde B, Eguía P, Stavroulakis GE, Granada E. Parameter identification for damaged condition investigation on masonry arch bridges using a Bayesian approach. Eng Struct 2018;172:275–84. https://doi.org/10.1016/j.engstruct.2018.06.040.
[88] Robert CP, Casella G. Monte Carlo Statistical Methods. 2nd ed. New York: Springer Series in Statistics; 2004.
[89] Palomo J, Paulo R, García-Donato G. Save: An R package for the statistical analysis of computer models. J Stat Softw 2015;64(13):1–23. https://doi.org/10.18637/jss.v064.i13.
[90] P. R. Wagner, J. Nagel, S. Marelli, and B. Sudret, "UQLab user manual–Bayesian inversion for model calibration and validation," *Chair Risk, Saf. Uncertain. Quantif. ETH Zurich, Switz.*, 2019.
[91] Goodman J, Weare J. Communications in Applied Mathematics and Computational Science. Commun Appl Math Comput Sci 2010;5(1):1–99.